SUBMITTED TO QJRMS

Convective Organization and Eastward Propagating Equatorial Disturbances in a Simple Excitable System

Geoffrey K Vallis[1] | **James Penn**[1]

[1]Department of Mathematics, University of Exeter, Exeter, EX4 4QF , UK

[1]g.vallis@exeter.ac.uk

11 March, 2020

We describe and illustrate a mechanism whereby convective aggregation and eastward propagating equatorial disturbances, similar in some respects to the Madden–Julian oscillation, arise. We construct a simple, explicit system consisting only of the shallow water equations plus a humidity variable; moisture enters via evaporation from a wet surface, is transported by the flow and removed by condensation, so producing an anomaly in the height field. For a broad range of parameters the system is excitable, even if linearly stable, with condensation producing convergence and gravity waves that, acting together, trigger more condensation. On the equatorial beta-plane the convection first aggregates near the equator, generating patterns related to those in the Matsuno–Gill problem. However, the pattern is unstable and more convection is triggered on its eastern edge, leading to a self-sustaining precipitating disturbance that progresses eastward. The propagation is eastward because the warm, moist converging air from the east induced by the Matsuno–Gill pattern is more convectively unstable than the converging air from the west. The pattern is confined to a region within a few deformation radii of equator, for here the convection can create the convergence needed to organize into a self-sustaining pattern; thus, smaller values of the beta parameter give rise to a wider disturbance. Formation of the disturbance preferentially occurs where the surface is warmer and sufficient time (typically a few tens of days) must pass before conditions arise that enable the disturbance to reform, a well-known characteristic of the MJO. The speed of the disturbance depends on the efficiency of evaporation and the heat released by condensation, and is typically a few meters per second, much less than the Kelvin wave speed.

1 | INTRODUCTION

Two, related, problems in tropical dynamics concern convective organization and the Madden–Julian oscillation (the MJO), both of which have been the subject of considerable investigation. However, no consensus has been reached in either case as to the key mechanisms involved and indeed, as recently as 2017, Fuchs and Raymond (2017) wrote that 'the MJO [has] been and still remains a "holy grail" of today's atmospheric science research'.

The MJO is a large-scale precipitating disturbance that propagates eastward at a few meters per second, centered near the equator and extending meridionally about 20° North and South (Madden and Julian, 1971; Zhang, 2005; Lau and Waliser, 2012). Its influence in the geopotential field extends zonally many thousand kilometers, and although the region of intense precipitation is confined to the tropics its influence can be felt in the mid-latitudes and stratosphere. Typically, the disturbance forms over the warm waters of the Indian Ocean and progresses east over the Maritime Continent and across the Pacific, decaying over the cooler waters of the eastern Pacific. The MJO reforms with a timescale of order a few tens of days – it is sometimes called the 30–60 day oscillation – and its spectral signature is manifest at a lower frequency than a Kelvin wave of the same scale (Wheeler and Kiladis, 1999; Kiladis et al., 2009). The MJO may be thought of as a translating disturbance that recurs on the above timescale, and that is the perspective we will take here.

The eastward propagation of the MJO suggests the influence of Kelvin waves, yet its propagation speed (around 5 m s^{-1}) is much less than that of dry Kelvin waves (about 20 m s^{-1}) for any reasonable equivalent depth of the atmosphere. The condensation of water vapor is likely to be a significant influence on the propagation of any precipitating disturbance and this led to theories centered around the notion of a 'moisture mode' (e.g., Raymond, 2001; Raymond and Fuchs, 2009; Sobel and Maloney, 2013). The framework of Majda and Stechmann (2009) also involves moisture in an essential way. Although the various models differ from each other in their assumptions and dynamics, a commonality is to assume some low-mode structure and calculate a dispersion relation or mode of instability that, depending on the form of the model, gives rise to propagation. Rather different types of model were presented by Biello and Majda (2005) and Yang and Ingersoll (2013), who suggested that the MJO is a multi-scale phenomenon with the convective structures resulting from a smaller scale activity.

In contrast to these relatively simple and/or semi-analytic models, comprehensive three-dimensional models are becoming able to simulate many aspects of the MJO (e.g., Liu et al., 2009; Nasuno et al., 2009; Holloway et al., 2013; Arnold and Randall, 2015; Khairoutdinov and Emanuel, 2018). In these simulations the MJO seems to be associated with some form of instability associated with a very large scale convective aggregation. However, the complexity of the models makes it difficult to determine the dominant mechanism and to make connections with or distinguish between the various simpler models.

Even without reference to the MJO, convective aggregation (e.g., Bretherton et al., 2005; Muller and Bony, 2015; Wing et al., 2017) is a fraught subject with a diversity of results across models and no single accepted dominant mechanism. 'Self'-aggregation, meaning the aggregation of convection over a surface of uniform temperature with no external large-scale influences, may be particularly sensitive to the parameters of the situation. However, as we will discuss, organization in a differentially rotating frame (essentially the beta plane) may be much more robust and may be the building block of the MJO.

In this paper we explore these issues and identify a robust mechanism of equatorial aggregation and eastward propagation. We do so through the use of a minimal but explicit model, specifically

the moist shallow water equations with relatively simple physics, a system that retains many of the properties of the three-dimensional equations. We try to make no assumptions that are not transparently connected to the properties of the equations of motions themselves. We find that the resulting system is an excitable one that, even when linearly stable, can produce self-sustained, irregular motion that, when solved on a beta-plane, gives rise to convective organization and eastward propagating equatorial disturbances with many similarities to the MJO. More generally, by considering tropical convection as an excitable system, properties that may have appeared surprising then seem less so, even where not fully understood.

We first describe the equations themselves. We then show the system admits of exact solution of no motion, and examine the stability and excitability properties of the system. After that we describe a number of numerical simulations and discuss the mechanisms of organization and eastward propagation. In the final section we place our results in a broader context and provide some conclusions.

2 | THE MOIST SHALLOW WATER EQUATIONS

The shallow water equations may be derived by way of an expansion of the hydrostatic primitive equations in terms of vertical modes (Matsuno, 1966; Vallis, 2017). The first baroclinic mode then obeys an equation set similar to the reduced-gravity shallow water equations albeit with some differences in interpretation – in particular the height field is related to the temperature field, and a heating is represented as a source or sink of mass. The usual derivation is valid only in the linear case, since the nonlinear terms bring in the interaction of additional vertical modes, but nonetheless equations of this general form are often regarded as good analogs of the primitive equations in cases when the vertical structure is dominated by the first baroclinic mode (e.g., Yano et al., 1995; Sobel et al., 2001; Majda and Stechmann, 2009). A deep first baroclinic mode is also an observed signature of the MJO (Kiladis et al., 2005; Adames and Wallace, 2014; DeMott et al., 2015).

We include moisture by introducing humidity variable, q, that is carried by the fluid and that is conserved in the absence of evaporation and condensation, and when condensation occurs it provides a heat source that affects the height field. Since moisture has a much smaller scale height than the troposphere (about 2 km rather than 8 km) we take the velocity field to be that of the lower atmosphere. The equations of motion then become, written using standard shallow water notation and omitting frictional and diffusional terms,

$$\frac{\mathrm{D}\boldsymbol{v}}{\mathrm{D}t} + \boldsymbol{f} \times \boldsymbol{v} = -g\nabla h, \tag{1a}$$

$$\frac{\partial h}{\partial t} + \nabla \cdot (h\boldsymbol{v}) = -\gamma C + R, \tag{1b}$$

$$\frac{\partial q}{\partial t} + \nabla \cdot (q\boldsymbol{v}) = E - C, \tag{1c}$$

where E represents evaporation, C represents condensation, R represents thermal forcing (e.g., a radiative relaxation) and γ is a parameter proportional to the latent heat of condensation. With no evaporative or thermal relaxation terms, but even in the presence of condensation, (1b) and (1c) combine to give the conservation equation

$$\frac{\partial M}{\partial t} + \nabla \cdot (M\boldsymbol{v}) = 0, \tag{2}$$

where $M = h - \gamma q$ is an analog of a moist static energy or equivalent potential temperature for the system. The above moist shallow water (MSW) equations are similar to those used by Bouchut et al. (2009) and Rostami and Zeitlin (2018), although the implementation and the experiments, described below, significantly differ.

Evaporation from a wet surface is parameterized by a bulk-aerodynamic-type formula,

$$E = \lambda |\boldsymbol{v}/U_0|(q_g - q)\mathcal{H}(q_g - q), \tag{3}$$

where λ is a constant (similar to a drag coefficient) and q_g is the surface humidity. The Heaviside function, $\mathcal{H}$, ensures that evaporation only occurs when the surface humidity is larger than that of the atmosphere, and dew formation is forbidden. The dependence on velocity ($|\boldsymbol{v}|/U_0$, where U_0 is a scaling constant) enables wind-induced evaporative effects to occur, and may be omitted.

Condensation is allowed to occur on saturation and we take it to be 'fast', meaning that it occurs on a timescale faster than any other in the system and does not allow the fluid to become significantly supersaturated. We represent this as

$$C = \mathcal{H}(q - q^*)\frac{(q - q^*)}{\tau}, \tag{4}$$

where q^* is the saturation specific humidity and τ is the timescale of condensation, and $\mathcal{H}$ is again the Heaviside function. (Fast condensation is a simplification of 'fast autoconversion', commonly used in cloud resolving models.) Precipitation schemes of this form are a common feature of various idealized GCMs and simple (e.g., Betts–Miller and convective-adjustment style) convection schemes (e.g., Betts, 1986). More elaborate convection parameterization schemes do exist for the shallow water equations (Würsch and Craig, 2014) but here we avoid their use. An expression for q^* in terms of h is derived in the next section.

Equations (1), (3) and (4) form a complete set. We now discuss the form of equations that we numerically integrate and the values of the parameters in relation to the true atmosphere.

2.1 Linear Equations of Motion

We will use the linear form of the momentum and height equations, but keep the nonlinearity in the moisture and Clausius–Clapeyron equations. The reason for this is that our main focus is on equatorial dynamics and the linear shallow water equations are remarkably fecund source of knowledge in that arena, beginning with Matsuno (1966) and Gill (1980). Tropical cyclones are also (deliberately) eliminated by such a linearization. However, a comparable linearization of the moisture equation, about either an unsaturated or saturated state, would be a poor approximation because of the large range of moisture values and the spatial variation of q^*, and convective triggering by a cold gravity wave be misrepresented. Since q and q^* do vary, it is not the case that moisture convergence alone leads to a convective instability.

The equations of motion become

$$\frac{\partial \boldsymbol{v}}{\partial t} + \boldsymbol{f} \times \boldsymbol{v} = -g\nabla h + \nu_u \nabla^2 \boldsymbol{v}, \tag{5a}$$

$$\frac{\partial h}{\partial t} + H\nabla \cdot \boldsymbol{v} = -\gamma C + \frac{(h_0 - h)}{\tau_h} + \nu_h \nabla^2 h, \tag{5b}$$

$$\frac{\partial q}{\partial t} + \nabla \cdot (q\boldsymbol{v}) = E - C + \nu_q \nabla^2 q, \tag{5c}$$

where H is the equivalent depth of the basic state and h is now the deviation from this. (Only the product of g and H is relevant to the dynamics, not g and h separately, but we retain familiar shallow water notation.) The term $(h - h_0)/\tau_r$ represents a radiative relaxation back to a prescribed value h_0 (usually taken to be zero) on a timescale τ_r, and we include diffusive terms with obvious notation.

2.1.1 Parameters and Relation to Atmosphere

Temperature variations may be roughly related to height variations by $h/H \sim -\Delta T/T_0$ where T_0 is a constant (e.g., 300 K), and we choose $H = 30\,\mathrm{m}$ and $g = 10\,\mathrm{m\,s^{-2}}$ (e.g., Kiladis et al., 2009). An appropriate radiative relaxation timescale τ_r is of order a few days, appropriate for a lower atmosphere (e.g., Gill, 1980). We do not include drag on velocity in the simulations shown here, but simulations with a moderate drag are similar. The coefficient of evaporation λ is such that for a typical velocity (which is of order $1\,\mathrm{m\,s^{-1}}$), or with no velocity dependence, the system becomes saturated in a few days. The diffusive parameters (ν_u etc.) are chosen on a numerical basis.

To obtain an appropriate expression for saturation humidity for use in (4) we begin with the approximate solution of the Clausius–Clapeyron equation, namely

$$e_s = e_0 \exp\left[\frac{L}{R^v}\left(\frac{1}{T_0} - \frac{1}{T}\right)\right] \approx e_0 \exp\left[\frac{L\Delta T}{R^v T_0^2}\right], \tag{6}$$

where e_s is the saturation vapor pressure, e_0 is a constant, R^v is the gas constant for water vapor, and $\Delta T = T - T_0$. Now, since the saturation specific humidity varies approximately in the same way as the saturation vapor pressure, we can write an expression for the saturation humidity in our system as

$$q^* = q_0 \exp(-\alpha h/H), \tag{7}$$

where $\alpha \sim L/(R^v T_0)$. With $R^v = 462\,J\,\mathrm{kg^{-1}\,K^{-1}}$ and $T_0 = 250\,\mathrm{K}$ we have $\alpha \sim 20$. Rather larger values are arguably more realistic since the shallow water equations mainly represent horizontal variations of temperature. We may take q_0 to be unity since it only appears in combination with the latent heat of condensation parameter γ.

To obtain an estimate for γ, note that in an ideal gas the latent heat of condensation, L, is such that $L\Delta q_a = c_p \Delta T$ where q_a is the specific humidity in the gas and c_p is the heat capacity at constant pressure. Here the analogous relation is $\gamma \Delta q = -h$ and so we estimate γ by

$$\gamma \sim \frac{LHQ_a}{q_0\, c_p T_0} \sim 8.5\,\mathrm{m}, \tag{8}$$

where Q_a is a typical saturated value of specific humidity near the surface in the tropical atmosphere and $q_0 = 1$. Using $L = 2.4 \times 10^6\,\mathrm{J\,kg^{-1}}$, $c_p = 1004\,\mathrm{J\,kg^{-1}\,K^{-1}}$, $Q_a = 0.035$, $T_0 = 300$ and $H = 30\,\mathrm{m}$ gives this value above.

All these parameter estimates are manifestly approximate, and variations of up to an order of magnitude may be reasonably explored. (Indeed, other implementations of the moist shallow water equations (e.g., Rostami and Zeitlin, 2018) use a fixed value of the saturation humidity.)

The above MSW equations thus include the effects of evaporation, transport and precipitation of moisture, the heat release associated with precipitation, and a temperature dependent saturation mixing ratio – some of the main features of a tropical atmosphere. Tropical convection is often described as having quasi-equilibrium nature on sufficiently long time scales (e.g., Betts, 1973; Arakawa and Schubert, 1974; Emanuel et al., 1994), associated with the convection occurring on a much faster timescale than that of the larger scale flow. The production of convective available potential energy (CAPE) by large-scale flow is then nearly balanced by the relaxation of CAPE by convection and the temperature profile is constrained to be close to neutrally stable. These effects are represented in our model by the use of a prescribed vertical structure and by condensational effects acting on a fast timescale. Convective instability will result if the fluid is near to saturation and the large-scale flow is convergent at the same location. However, convergence alone does not necessarily lead to convection, nor is convergence the only way to excite it; gravity waves can also trigger convection given the height dependence of the Clausius–Clapeyron equation.

3 | STEADY SOLUTIONS, STABILITY AND EXCITABILITY

In a state of no motion the height and moisture equations are, neglecting horizontal diffusion,

$$0 = -\gamma C - \lambda_r h, \tag{9a}$$

$$0 = \lambda(q_g - q)\mathcal{H}(q_g - q) - C, \tag{9b}$$

where $\lambda_r = 1/\tau_r$, the condensation C is given by (4) and the saturation humidity is given by (7). In the Appendix we find the exact, analytic solutions to these equations.

If $q_g \le q_0$ the solution has $h = 0$, $q = q_g$, $C = 0$ (because $q \le q_*$) and zero evaporation. If $q_g > q_0$ then there is evaporation from the surface, balanced locally by condensation. This is a 'drizzle solution', and in the height equation the heat released by condensation is balanced by radiative damping. The first, unsaturated case will be linearly stable (i.e. stable to infinitesimal perturbations), and the system will relax back to the initial state. But in the drizzle solution a small perturbation will trigger more condensation and latent heat release, and the perturbation may grow, as discussed more below.

Both types of solutions can be expected to be conditionally unstable, unless the diffusive and damping terms in the equations are very strong, as can be seen by the following argument. If $q_0 \le q_g$ then the solution is such that atmosphere is saturated. A localized perturbation, even an infinitesimal one, will in general lead to further condensation and thence a perturbation in the height equation and the generation of gravity waves, as well as low-level convergence at the source of condensation. These gravity waves will propagate and will induce more condensation nearby, which will in turn generate more gravity waves and so on. Evidently, unless the damping is large, the steady saturated solution is unstable. If, on the other hand, $q_0 > q_g$ then the steady solution will not be saturated and an infinitesimal perturbation will have little effect. Nevertheless, a finite-amplitude perturbation large enough to trigger condensation may generate further motion, more condensation and so on. Thus, unless the damping is very large any perturbation that causes

saturation will lead to the generation of motion and a spreading field of precipitation as the gravity waves propagate.

Following a perturbation, and depending on (a) the rate of evaporation from the surface, (b) the magnitude of the latent heat of condensation, and (c) the size of the damping terms, the system will either evolve into a sustained convective state, or the perturbations will eventually die and the system will return to a state of no motion. The return can occur, even if the initial state is linearly unstable, because the precipitation occurs at a lower temperature than that of the drizzle solution, leaving the atmosphere unsaturated and non-precipitating as it slowly relaxes back to the initial state. The moisture is slowly replenished by surface evaporation, but if that occurs on a timescale that is long compared that on which the gravity waves are damped then the atmosphere only reaches saturation when all the perturbations have died. An external perturbation could nevertheless excite the system again.

On the other hand, with sufficiently small damping and sufficient latent heat release the system will evolve to state of self-sustained motion; that is to say, the system will be 'excitable'. Various forms of excitable system exist (e.g., networks of neurons, auto-catalytic chemical reactions, certain cellular automata) and there is no universal definition, but typically they are extended non-equilibrium systems that may have a linearly stable fixed point but that nevertheless are susceptible to finite perturbations (Meron, 1992; Izhikevich, 2007). In our system, the return or otherwise to the initial state does not directly depend on the linear stability properties of the initial state: numerical experiments show that self-sustained states of convection may exist even if $q_0 > q_g$, in which case the steady solution is not saturated and thus linearly stable, and the sustained convection is then subcritical. Conversely, if the damping is moderately large, the system may return to its initial state, and stay there, even if that state is saturated and linearly unstable.

3.1 Marginal excitability

A typical evolution in physical space from the initial state for an excitable state is shown in Fig. 1. A small localized perturbation is applied that triggers convection, and sends out a gravity wave, leading to more convection and precipitation and a propagating, precipitating front. Initially the front is nearly circular but later breaks up into smaller fronts that in turn propagate with no preferred direction (in the absence of differential rotation) and decay, each one triggering convection nearby. In the excitable regime the convection continues indefinitely (as in this figure).

The evolution from the small perturbation is characterized by an initial spike in the energy (see Fig. 2b), a common feature of excitable systems (e.g., figure 7.1 of Izhikevich (2007)), followed either by a return to the initial state, (typically on a timescale of tens of days) or by self-sustained motion. There is no analytic theory (to the authors knowledge) that determines the boundary between the stable and excitable regimes, and quantitative results must be obtained numerically, as illustrated in Fig. 2a. To determine the boundary the equations are numerically solved in a domain of size 10^4 km in both x- and y-directions, periodic in the x-direction and with a sponge near the meridional walls, and no rotation. (In later simulations with a nonzero beta the equator is in the center at $y = 0$.) In each case we choose $q_0 = q_g$, meaning that the state with no motion is just saturated and marginally unstable, by analogy to the tropical atmosphere (Xu and Emanuel, 1989). From that state, and for each set of parameters, a small perturbation is added and the system allowed to evolve freely. The system will either evolve into a self-sustained state or, after some time, return to its initial (unperturbed) state. Depending on the result of a particular experiment the damping and/or rate of evaporation is increased or decreased until a marginally critical state is found, and each black dot in Fig. 2 represents the convergence of such a process. There is an almost inverse

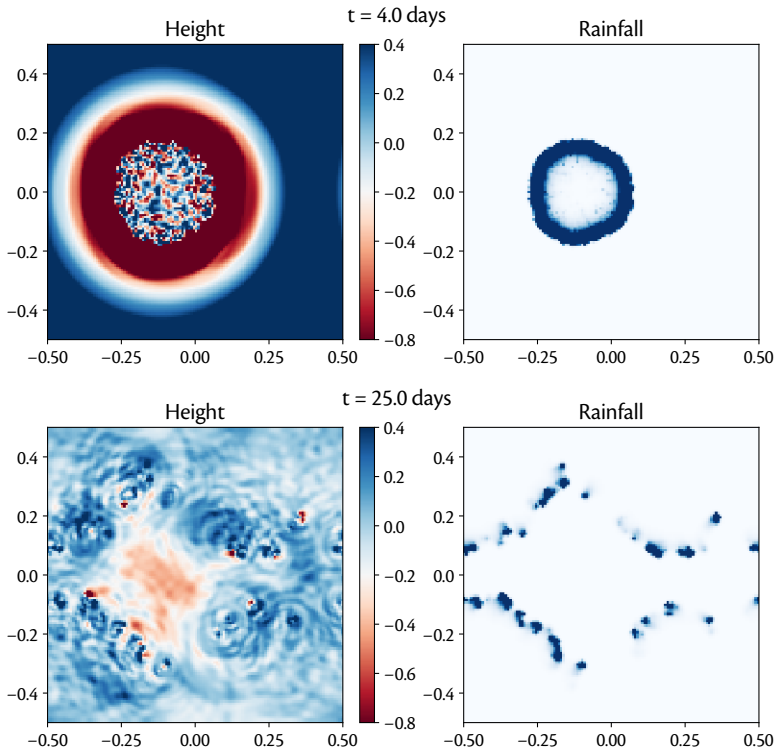

FIGURE 1 Snapshots of the height and precipitation fields at the times indicated, following an initial small perturbation at $y = 0$ and $x = -0.1$. (Units of x and y are 10^7 m, and the precipitation field is slightly smoothed in space and time and uses a near-binary colour map.) The disturbance generates a front that propagates away from the disturbance before breaking up, then continuing in excitable, self-sustained motion. By time 25 the precipitation fronts are propagating quasi-randomly though the domain, breaking up and reforming every several days.

relation between the critical values of the radiative damping and the evaporation rate; that is, higher values of radiative damping require a larger rate of evaporation to maintain excitability. The other important moisture parameter is the latent heat of vaporization, γ, and the dependence of kinetic energy on γ, once the system reaches statistical equilibrium, is shown in Fig. 2c. The system is largely driven by the release of latent heat and the kinetic energy increases approximately linearly with γ. Similar behavior occurs for a range of values of α from 10 to 100, and here we use $\alpha = 60$, and there is no velocity dependence in the evaporation.

Conditional instability is the building block of excitability in the real atmosphere and the ability of the atmosphere (and three-dimensional models) to produce propagating convective activity depends on the ability, or otherwise, of localized convection to trigger and organize convection nearby and hence produce self-sustaining motion. If convection triggers more convection nearby, convective aggregation can ensue. The real world may not lack for perturbations to initiate convection if the basic (radiative-equilibrium) state is conditionally unstable, and gravity waves from existing convection being one such perturbation. The convection also needs to produce an anomaly in the geopotential field of sufficient magnitude to organize the flow if convective patterns such as the MJO are to be produced, and we now show how differential rotation can do just that.

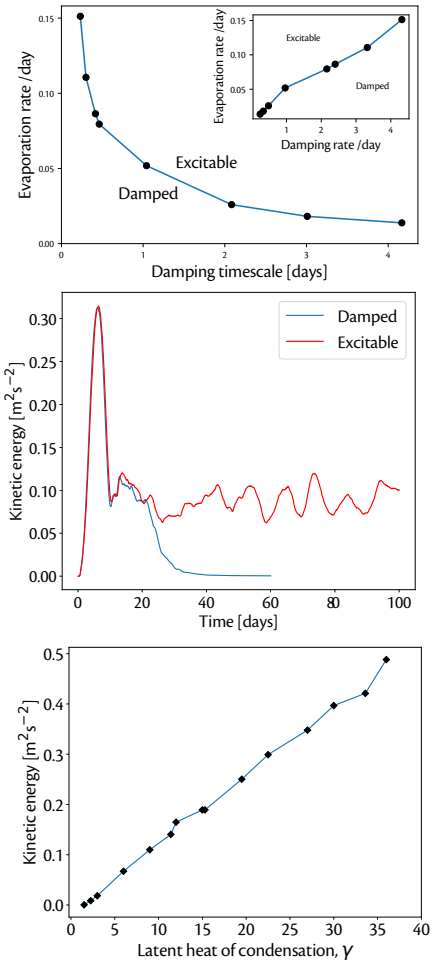

FIGURE 2 (a) Boundary of the excitable state for varying values of the radiative damping of the height field and the efficiency of evaporation. The stationary state is saturated with no precipitation of evaporation. In the excitable regime the system maintains a chaotic, convectively active state. In the stable state the system eventually returns to its original state of no motion, even though that state is linearly unstable. (b) Evolution in excitable and a damped states, both with a damping timescale of 2 days and with evaporative parameters on either side of the critical line. (c) The domain and time-averaged kinetic energy as a function of the latent heat parameter, γ.

4 | EFFECTS OF ROTATION

We now explore the effects of rotation on the system. We first briefly discuss the case with constant rotation (i.e., flow on the f-plane) and then, in more detail, the case on a beta-plane.

4.1 Flow on the f-plane

We apply a constant rotation of $f = 1 \times 10^{-4}$ s^{-1} and the perform experiments otherwise identical to those shown in Fig. 1. The initial evolution is very similar, but after a few days it is quite different, for the planetary rotation mitigates *against* the organization of the convection. The reason is that the velocity induced by the condensational heat source tends to give rise to rotational motion around the

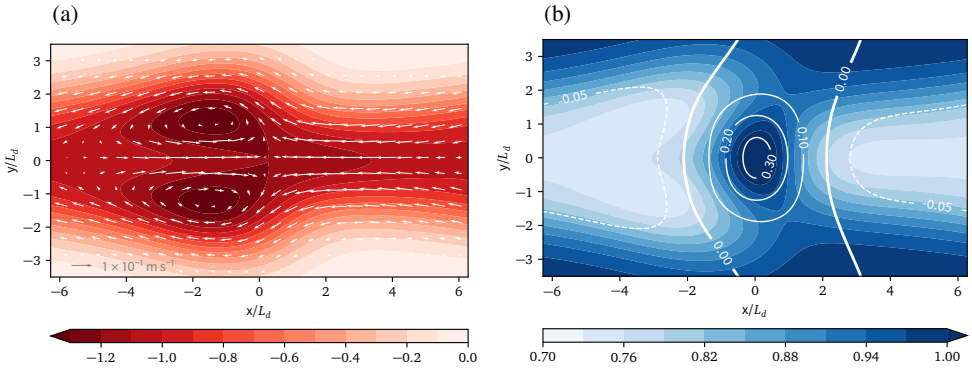

FIGURE 3 Response to a steady heating centered at the origin on an equatorial beta-plane, where moisture is a passive tracer. (a) The height field (color filled contours) and wind vectors (arrows). (b) The absolute humidity (specifically $q/q_0 - 1$, white contours) and relative humidity q/q^* (color filled contours), with darkest blue indicating saturation.

heat source because of the tendency toward geostrophic balance, rather than convergence toward it. (The effect is well illustrated by moving the heat source away from the equator in the Matsuno–Gill problem, as illustrated in figure 8.14 of Vallis, 2017.) This result should not be taken to mean that convective organization is impossible in the presence of rotation, since the omission of the nonlinear terms in the momentum equation means that, among other things, shallow water cyclones do not form.

4.2 Flow on a beta plane

To understand flow on a beta plane we first consider the case with humidity as a passive tracer, with no latent heat release, before considering the case where humidity feeds back on the flow.

4.2.1 Humidity as a passive tracer

We set $\gamma = 0$ in (5) but otherwise keep the equations unaltered, so that moisture evaporates from a saturated surface, is advected by the flow and condenses upon saturation. We integrate the equations on an equatorial beta-plane with $f = f_0 + \beta y$, with $f_0 = 0$ and $\beta = 2 \times 10^{-11}$ m^{-1} s^{-1}. The flow is forced by a static heating in the center of the domain of the form

$$Q = h_0 \exp\left(-\frac{x^2 + y^2}{L_d^2/2}\right). \tag{10}$$

where h_0 is a constant. The flow itself organizes into a familiar, steady, Matsuno–Gill-like pattern, illustrated in Fig. 3, with convergence very near to the center of the heating, depending slightly on the drag and relaxation parameters. Whereas moisture accumulates near the center of the heating, it is the relative humidity that determines whether condensation occurs and this is a function of the height field as well as moisture. The large-scale warm anomalies of the Rossby lobes west and slightly poleward of the heating, and the Kelvin waves east of the heating, inhibit precipitation except in regions close to the heating.

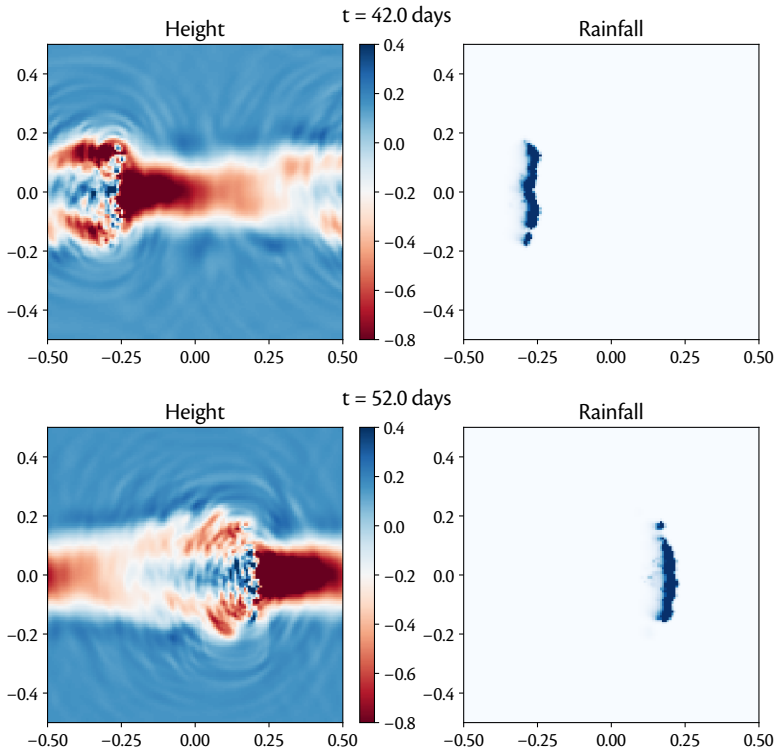

FIGURE 4 Snapshots of the height and precipitation fields at the times indicated, in simulations on a beta plane, with $\beta = 2 \times 10^{-11}$ m^1 s^{-1}, a resolution of 25 km and no imposed mean flow. The main disturbance forms about 30 days after initialization and propagates eastward at about 6 m s^{-1}. Units of x and y are 10^7 m and the equatorial deformation radius is about 10^6 m.

Although there is a relative drying out of the equatorial region far to the east of the forcing, in the direct vicinity of the forcing the peak of relative humidity maximum is actually slightly to the east of the forcing center because of the asymmetry in the Matsuno–Gill pattern. The moisture convergence thus gives rise to condensation slightly east of the original heat source, so providing a new heat source. This in turn creates a pattern slightly east of the original one, and so on, thus potentially providing a basic mechanism for steady eastward propagation. If moisture is made to be an active tracer the flow becomes unsteady and propagates east, as we now explore.

4.2.2 Humidity as an active tracer

We now describe some simulations on the beta plane in which moisture is an active tracer, with condensation leading to latent heat release and producing a height anomaly. The initial evolution from a localized perturbation is similar to that in the non-rotating case shown in Fig. 1. At subsequent times rotational effects inhibit the aggregation of convection in mid-latitudes, but close to the equator the convection organizes itself. Condensation near the equator provides a heat source, which tries to generate a pattern similar to that of the left panel of Fig. 3, with moisture convergence maintaining the heat source. Unlike the case with no rotation, there is an east-west asymmetry, for two related reasons. First, the Matsuno–Gill pattern itself is asymmetric, bringing warm, moist air from the east. The associated convergence leads to condensation on the leading (i.e., eastern)

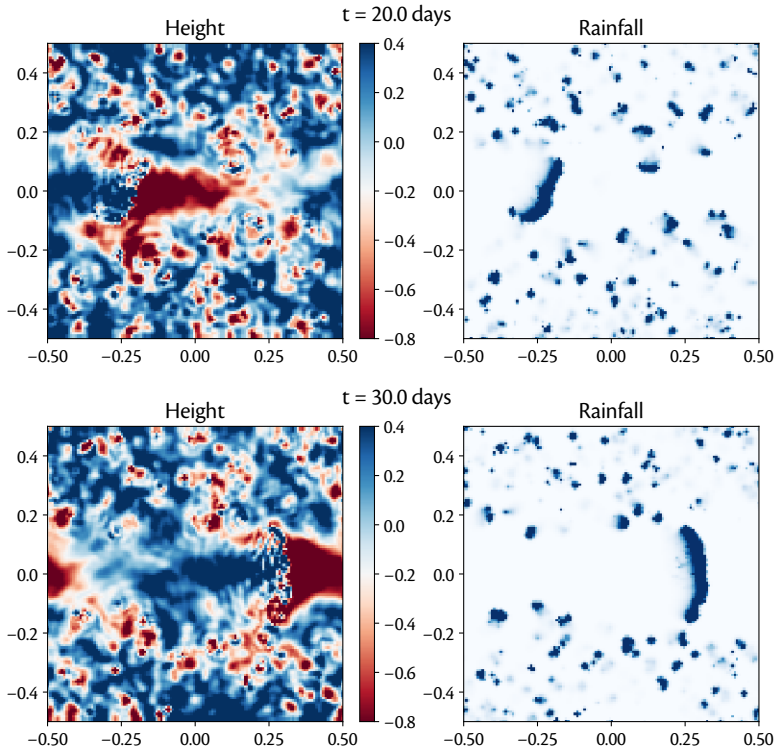

FIGURE 5 As for Fig. 4 except that a mean westward flow of 1 m s^{-1} is included in the bulk-aerodynamic formulation of evaporation.

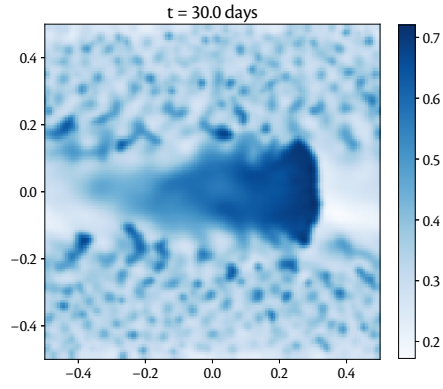

FIGURE 6 Snapshot of evaporation field (normalized by its maximum value) in the simulation of Fig. 5. The evaporation is less ahead of (i.e. east of) the main convective region.

edge of the existing condensational heat source, leading to the formation of a precipitating front, related to those described by Frierson et al. (2004) and Lambaerts et al. (2011). Second, close to the equator Kelvin waves are excited and these propagate east, triggering convection and generating more convection in the moist converging fluid just east of the initial disturbance, and so on. If the system is excitable the mechanism is self-sustaining and the precipitation front propagates

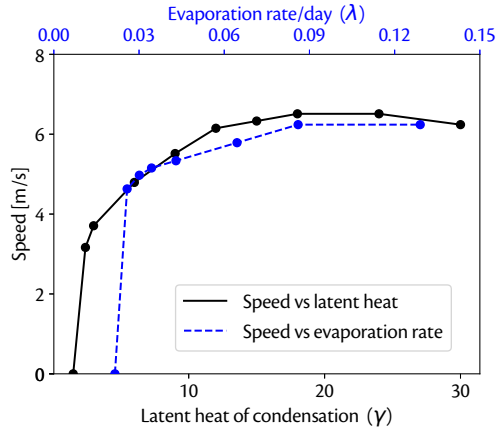

FIGURE 7 Speed of the main, MJO-like, eastward moving disturbance as function of the evaporation coefficient λ and the latent heat of condensation, γ. Where γ varies the value of λ is fixed at 0.08 and when λ varies the value of γ is 15.

eastward. A typical progression are shown in Fig. 4; the simulation has $\alpha = 60, \gamma = 15, \tau_r = 2$ days, $\lambda = 0.08\,\text{days}^{-1}, \beta = 2 \times 10^{-11}\,\text{m}^{-1}\,\text{s}^{-1}$ and a resolution of 20 km. Simulations with resolutions from 80 km to 10 km show very similar behavior. The simulation in Fig. 5 is the same except that a mean westward wind of $1\,\text{m}\,\text{s}^{-1}$ is added to the evaporation formulation, discussed further in Section 5.2. The associated height pattern is qualitatively similar to a Matsuno–Gill pattern with a warm, leading Kelvin lobe eastward of the precipitation and confined to the equatorial region, and Rossby lobes flanking and slightly westward of the precipitation.

Although the structures in these figures are overly idealized, they are broadly consistent with the patterns seen in observations (e.g., Kiladis et al., 2005; Adames and Wallace, 2014). Different parameter choices give rise to somewhat different shapes, and on some occasions the Kelvin lobe itself is flanked by geopotential disturbance of opposite sign, giving a quadrupole nature to the height field, but the approximate swallowtail-like structure in the height field and mechanism of propagation remain robust to parameter choices. Evaporation (see Fig. 6) is smaller on the eastern side of the front and this is because the air is already moist there; that is to say, the build up of moisture in the main convective region is not a consequence of local evaporative anomalies. Consistently at least, De Szoeke et al. (2015) find that it is moisture convergence, and not evaporation anomalies, that contributes most to moisture budget during observed MJO events.

The speed of the disturbance is not directly associated with the dry gravity wave speed, or even a moisture-modified gravity wave. Rather, it is associated with the time taken for the circulation to respond to a heat source: the disturbance cannot move so quickly that the Matsuno–Gill-like pattern cannot keep up with it and maintain a westward wind with a supply of water vapor. The strength of the pattern, and thus its timescale, is determined by the release of latent heat, and as Fig. 7 shows the speed increases as either the latent heat of condensation increases or as the efficiency of evaporation increases. The speed does not increase without bound, for as the influence of moisture increases the pattern formation becomes more irregular, and two or more precipitating patterns may form along the equator, each stealing moisture from the other and slowing the propagation. For still higher values the system can become too excitable; the convection then occurs too randomly and no discernible MJO-like pattern arises.

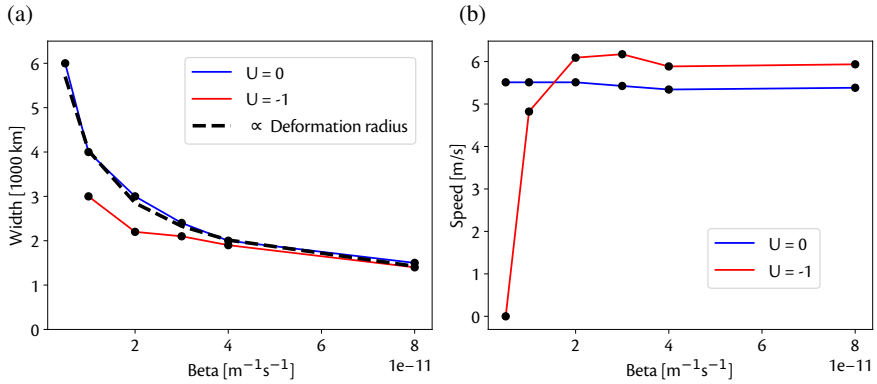

FIGURE 8 (a) Width of the precipitating region as a function of β. The deformation radius, $\sqrt{c/2\beta}$ is about 700 km in the these experiments. The two solid curves show a sequence of experiments with $U = 0$ and $U = -1\,\mathrm{m\,s^{-1}}$, where U is the speed of the imposed mean flow affecting the evaporation. The dashed line shows a curve proportional to $\beta^{-1/2}$. (b) Same as (a), except now for the speed of the disturbance. For $\beta = 0.5 \times 10^{-11}$ no MJO-like phenomena is obtained in the case with $U = -1$.

4.2.3 Scale dependence on β

The scale of organization of flow on an equatorial beta-plane is largely determined by the equatorial deformation radius, $L_d = (c/2\beta)^{1/2}$, where c is the speed of the gravity waves. The meridional scale of the Matsuno–Gill pattern is about 5 deformation radii and the zonal scale is two or three times larger than that. For $c = 20\,\mathrm{m\,s^{-1}}$ and $\beta = 2 \times 10^{-11}\,\mathrm{m^{-1}\,s^{-1}}$ we have $L_d = 700\,\mathrm{km}$ and thus the meridional scale of organized disturbances can thus be expected to be a few-to-several thousand kilometres.

The latitudinal width of the precipitating disturbances in our system does indeed scale quite well with the deformation radius. The results of a sequence of experiments with varying values of β and fixed c, with and without an imposed mean flow, are shown in Fig. 8a. For latitudes beyond a few deformation radii from the equator the convergence is too weak to generate an organized pattern, as in the f-plane simulations. However, the speed of the disturbance, provided that an organized pattern forms, varies very little. Although the disturbance is wider for smaller beta, the intensity of the flow in the region of the disturbance does not vary significantly, being a much stronger function of the latent heat parameters, as in Fig. 8b. For still smaller values of beta than those shown no coherent structure robustly forms in the domain.

5 | PROPERTIES AND FEEDBACKS

In this section we look at various other effects influencing the model behaviour, in particular the sea-surface temperature, wind-induced evaporation, cloud-radiative effects and mdel resolution.

5.1 Reccurrence Period and Effect of Varying SST

A well-known feature of the MJO is that it forms over the warm waters of the Indian Ocean, and that the next event formation will occur some 30–60 days later. It is, in fact, a common feature of an excitable system that it cannot support the passage of a second disturbance over a given

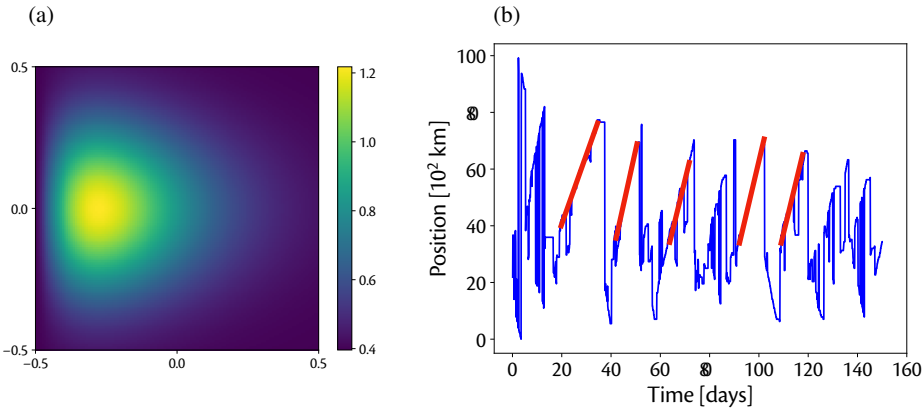

FIGURE 9 (a) Sea-surface humidity, representing a warm pool in the western equatorial region with a fractional humidity about 25% above a base level (b) Position of the maximum precipitation at the equator, with thicker red lines indicating where the precipitation is associated with MJO-like activity. MJO events form only in the warm western region and decay before reaching the eastern edge, and here recur every 20–40 days.

location until sufficient time – the 'refractory period' – has passed (Izhikevich, 2007), and this is also a property of our model. To demonstrate this we impose a spatially varying distribution of surface humidity, as one would find with a varying sea-surface temperature anomaly, as in the left panel of Fig. 9. The right panel shows the position of the main disturbance, as determined by the location of the maximum of the precipitation divergence in the velocity field. Disturbances typically form only in the vicinity of the maximum surface humidity and propagate east, decaying where the surface humidity is too low. A second disturbance cannot form until the first disturbance is sufficiently distant from the genesis location, because the first disturbance leaves a wake of dry air that needs sufficient time to reform into a converging pattern and initiate the moisture feedback. In the simulation shown the reformulation time is roughly 20-40 days, the time taken for an MJO disturbance to fully clear the genesis region and for a new pattern to reform. Note that even without a previous MJO disturbance the atmosphere typically takes many days to organize itself into a quasi-steady state in response to a localized heating (Heckley and Gill, 1984).

5.2 Wind-induced evaporation

The effect of wind-induced evaporation is sometimes mentioned as a possible mechanism for influencing the larger-scale flow and enhancing eastward propagating disturbances (e.g., Neelin et al., 1987; Emanuel et al., 1987). In our numerical experiments we find that the robustness of the formation of a coherent equatorial structure and its eastward propagation can be enhanced by the presence of a wind-evaporation feedback, but the eastward propagation (on the equatorial beta-plane) does not rely on that effect. Specifically, suppose evaporation, E, is parameterized via a term of the form

$$E = \lambda \frac{|\boldsymbol{v} + \boldsymbol{U}|}{U_0}(q_0 - q), \tag{11}$$

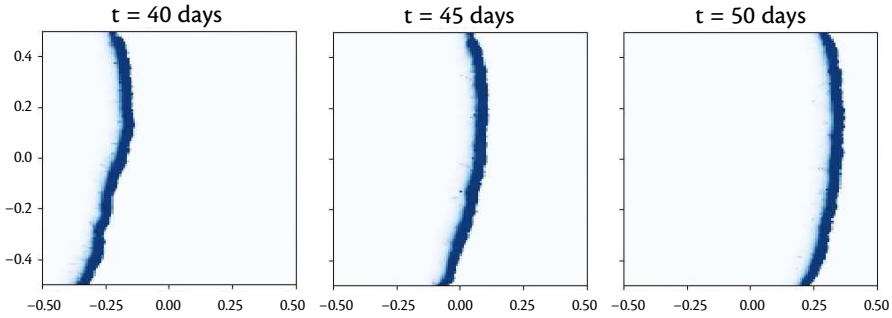

FIGURE 10 Rainfall at the times indicated in a simulation with no rotation, $f = \beta = 0$, but with an imposed uniform westward mean flow of $1\,\mathrm{m\,s^{-1}}$ in the bulk formula for the evaporation, (11). This term is the only one in the system that imposes a mean direction. The speed of the front here is about $5\,\mathrm{m\,s^{-1}}$.

for $q_0 > q$, and where v is the model produced wind and U is a constant, background wind due to, say, the trades. If U is directed westward, then evaporation is enhanced eastward of the disturbance and, if $|U| \approx 1\,\mathrm{m\,s^{-1}}$ (similar to wind speeds produced internally by the disturbance itself) the formation of an eastward propagating disturbance occurs over a somewhat broader range of parameters but, as is apparent from figures 4 and 5, eastward propagation can occur without the enhanced wind-induced evaporation. On the other hand, if U is eastward with a similar magnitude then eastward propagating MJO-like disturbances are found to be eliminated.

Having said this, eastward propagation can occur even in $\beta = 0$ in the presence of a wind-induced evaporative effect. If simulations are performed with $U = 0$ and with $f_0 = \beta = 0$, then fronts form intermittently and move with no preferred direction, typically breaking up and reforming later, depending on the parameters, and so the excitability, of the system (as in the bottom panels of Fig. 1). If a mean flow is now imposed (but still with $f_0 = \beta = 0$) then the fronts that form will, after maturation, move eastward or westward, depending on whether U is directed westward or eastward, respectively, with a speed dependent on the magnitude of U. After sufficient time, the front will organize to span the entire domain and move steadily in the direction opposing that of U, as in Fig. 10. The speed of the front is a few times that of the mean flow, and is similar to the speed of the fronts the case with no mean flow. That is to say, the main effect of the mean flow is an organizing one.

5.3 Cloud–Radiation Interactions

Cloud–radiation interactions have been found to play a role in producing MJO-like patterns in both idealized models (e.g., Raymond, 2001) and some cloud-resolving models (e.g., Khairoutdinov and Emanuel, 2018). A feedback occurs because in the presence of precipitation clouds form and these reduce the atmospheric cooling, because the radiation to space occurs from a higher elevation and so a lower temperature; this in turn may lead to surface heat flux anomalies and instability (Raymond, 2001). Whether it is this same process that occurs in cloud-resolving models and GCMs is less clear but nevertheless the cloud-radiative effect can be expected to be at least a noticeable one, given that the cooling rate depends strongly on the emitting temperature. We can introduce a similar effect in our model by reducing the rate of radiative cooling when precipitation is present, with the lapse rate itself still presumed set by convection, although without a full radiative transfer model any prescription is perforce very approximate. For example, a straightforward way to include the effect

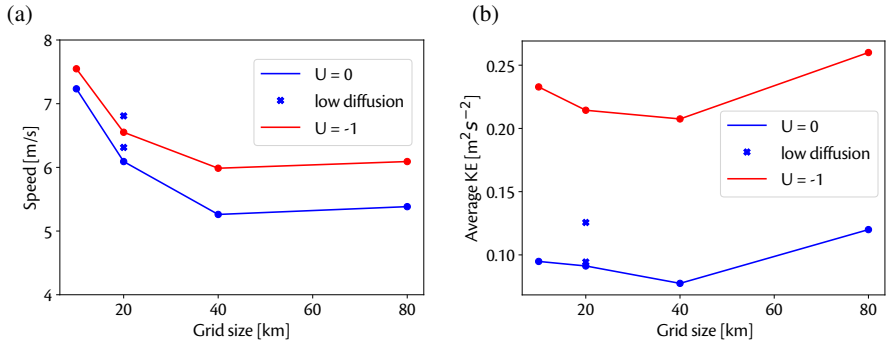

FIGURE 11 (a) Dependence on resolution of the speed of the moving disturbance. (b) Dependence on resolution of average kinetic energy of the system (over the whole domain). The blue and red lines show simulations without and with an additional mean westward flow of 1 m s^{-1} affecting the evaporation. The additional cross marks show simulations with values of the diffusivity of height, moisture and velocity further reduced by factors of 2 and 4, in simulations without the additional wind-induced evaporation.

is to let Cooling rate = Cooling rate (control) $\times$ [1 $-$ α Precip/max(Precip)] where 'Cooling rate (control)' is the linear relaxation term on the right-hand side of (5b). Such a scheme reduces the cooling by a factor of α over the strongest precipitation and has little effect elsewhere. We have performed several experiments with a term of this form, and we find that, similar to the results in Section 3.1, the effect is to dampen the system less and make it more unstable. The effect is not especially marked in the simulations we have performed, but it does slightly broaden the range of parameters that gives rise to an eastward propagating disturbance. If it is the case that many comprehensive models are on the borderline of producing MJOs, but perhaps are not sufficiently unstable to do so, then such an effect could certainly tip them into such a regime. However, it would not be correct to say that the cloud-radiative effect drives the disturbance; rather, it may enhance a form of instability that is necessary in order that eastward propagation can occur.

5.4 Effects of resolution

We have performed a sequence of simulations on the equatorial beta-plane with resolutions of 80 km, 40 km, 20 km and 10 km in a square domain of size 10,000 km by 10,000 km. All of them had the same physical parameters (the same as those used to give Fig. 4). Although instantaneous condensation tended to concentrate at the grid scale in all simulations, very similar large-scale behaviour occurred, and in particular the speed varied only rather slightly with resolution, as illustrated in Fig. 11. The large scale pattern and the variations in the height field are similar in all cases, and it is because it is the self-maintenance of this large-scale pattern that leads to its eastward propagation, the simulations give similar results. The kinetic energy also varies only by a relatively small amount with resolution for a similar reason. The addition of a uniform eastward flow in the evaporative scheme does increase the propagation speed slightly, and the average kinetic energy by a larger fraction. The increase in kinetic energy mainly occurs in midlatitudes, away from the equatorial organization; for without that effect there is very little convective organization in the mid-latitudes because of the inhibiting effects of planetary rotation, as mentioned earlier.

6 | DISCUSSION AND CONCLUSIONS

We have presented a simple, explicit model that reproduces many of the main features of intra-seasonal variability and the Madden–Julian oscillation in the tropical atmosphere, and described the mechanism that causes these features. By simple we mean that we treat the atmosphere as a single baroclinic mode in the vertical and we do not use any convective parameterization (except a rather basic one), and by explicit we mean we do not make additional approximations about the scale and nature of the system; rather, we directly solve the resulting equations of motion, which consist simply of the shallow water equations plus a humidity variable. Condensational heat release leads to an anomaly in the geopotential, which in turn induces a velocity field, leading to more convection and so on. If the condensational effects are sufficiently strong, as determined by the latent heat of evaporation and the efficiency of evaporation from the surface, and the radiative damping appropriately weak, the system is excitable and self-sustained motion ensues. Such behavior occurs over a wide range of physically reasonable parameters and in this regime the motion – which can develop quite large scales – is driven by the condensational heating at small scales; there is no large-scale modal instability.

When integrated on the beta plane the motion in the tropics becomes organized. In a background state that may be linearly stable the convection aggregates around the equator creating a Matsuno–Gill-like pattern with a scale determined by the equatorial deformation radius. However, the pattern is unstable to finite perturbations: the combination of moist convergence and gravity waves triggers convection nearby and the disturbance propagates, and does so preferentially in an eastward direction. The directionality arises because the pattern draws warm moist air in from the east along the equator, and this air becomes conditionally unstable. Convection is triggered at the eastern edge of the existing disturbance and the whole system then propagates east, as sketched in Fig. 12. Note that the moisture is not advected eastward in the disturbance; rather, it has an evaporative source and is drawn in *from* the east. The large-scale disturbance may be surrounded by a collection of smaller-scale convective events, and these have no preferred direction because the pressure field they induce is more nearly isotropic and there is no preferred instability on their eastern edge. The scale of the overall disturbance is set by the equatorial deformation radius, and thus of order a few thousand kilometres.

Although simple in construct, the model displays some of the key observed features of the spatial structure, scale and period of the Madden–Julian oscillation, notably:

1. A predominantly dipolar Matsuno–Gill-like pattern in the height field, sometimes called a swallowtail, with a Kelvin lobe extending east, flanked by two off-equatorial Rossby lobes to the west. The size of the structure depends on the equatorial radius of deformation.
2. The whole pattern moves eastward at a speed of a few meters per second. The speed is largely determined by the level of moisture in the system and by the magnitude of the latent heat of condensation, which determine the strength of the pattern and the time it can take to form and move itself. Isolated clumps of convection of various sizes may surround the central precipitating region.
3. The pattern preferentially forms where there is greater availability of moisture, corresponding to a higher sea surface temperature. If a pattern forms and moves east from that location then an interval of order a few tens of days must pass before a second disturbance can form in the dry wake of the first.

None of these features listed are built-in to the model; rather, they are all emergent properties.

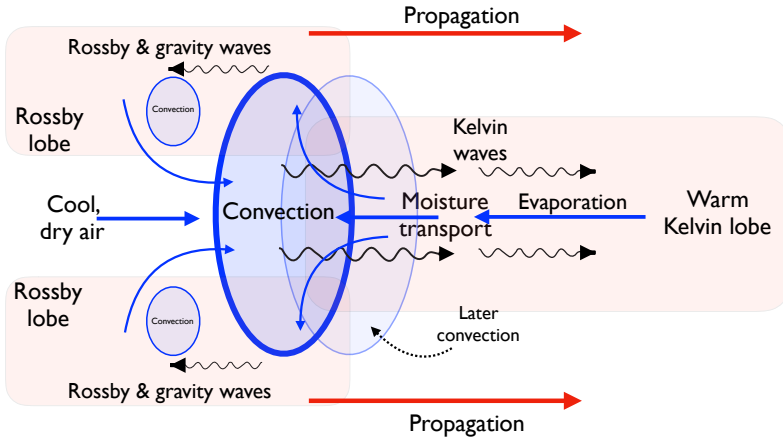

FIGURE 12 Schematic of an eastward propagating equatorial disturbance. Convection at the equator gives rise to a feedback producing convective organization and a modified Matsuno–Gill-like pattern. Warm moist air is then drawn in from the east but this is convectively unstable, amenable to triggering by the eastward propagating gravity waves from the initial disturbance, and new convection forms on the eastern edge of the original location. The whole pattern then moves unsteadily eastward.

although, à propos of point 1, a Gill response is very common for nearly any localized equatorial heating. A detailed comparison with observations is beyond the scope of this paper, but two other comparisons are worth mentioning.

First, a key feature of this model is that existing convection preferentially draws moist air in from the east, and it is because this air is conditionally unstable that convection occurs just east of the existing site, leading to propagation. Thus, humidity is higher east of the centre of convection than it is to the west, especially at lower levels, as in the schematic (Fig. 12). Consistently, the evaporation is actually smaller to east of the convective maximum than to the west (Fig. 6) because the air is already moist. The observations also show higher humidity east of the convective maximum: Fig. 13 shows the latitude-height section of relative humidity anomaly in a composite MJO event, using ERA-interim data from 1989 to 2008 and an index of outgoing longwave radiation as a proxy for convection and to identify MJO events. The events are composited and relative humidity averaged from 10° N to 10° S, and here day 0 corresponds to an event with convection peaking over the western Maritime Continent. A tongue of moist air is present at low levels east of the main convective region, and it is the presence of this air that leads to the eastward propagation of the convection. The relative humidity is high because the moisture is high (not because temperature is low), with the high moisture coming from the long fetch of the Kelvin mode east of the main convection centre.

Second, the asymmetry in the model, and the triggering of convection, occurs because of the eastward propagation of Kelvin waves. Although there are many triggers for convection in the real atmosphere, Wang et al. (2019) note that during propagating MJO evens there is a particularly strong coupling between the Kelvin wave response and the convection that is absent otherwise.

The presence of a wind-induced evaporation, or WISHE, does have an noticeable effect on its eastward propagation but the eastward propagation can also occur without mean easterlies — as is observed in the Indian Ocean where the surface winds are complex (e.g., Hastenrath and Polzin, 2004). Second, since the energy source is, ultimately, evaporation from the surface, a higher SST (i.e., a higher level of surface humidity) produces a more energetic simulation and is responsible

for the localization of the genesis region. A less realistic feature of the model is that the moisture convergence and feedback onto the height field lead to the formation of fronts that are very narrow in the along-propagation direction, compared to observations of composite MJOs. However, both observations from TRMM and high resolution three-dimensional simulations do show that the region of intense precipitation becomes meridionally extended and zonally confined as the MJO enters the western Pacific (Liu et al., 2009). Tight frontal formation is in fact commonly found in idealized moist systems (Yano et al., 1995; Frierson et al., 2004; Lambaerts et al., 2011), and the gridpoint generation of storms and fronts are also a common feature of moist models without a convective parameterization, and our model is no exception in that regard.

The interaction of the moisture field with the pressure and wind fields is essential to the mechanism we have presented here, as it is in the moisture-mode theories discussed in the introduction. However, our mechanism differs, or appears to do so, in key respects; in particular, the mechanism is not a mode of variability in the normal scientific sense of that word. It is of course possible that, after suitable averaging, our model could be reduced to a lower-order or quasi-linear model which resembles a moisture mode, but that is a task for another day. Perhaps, though, rather than model details it is the essential mechanism that ultimately matters. We propose that large-scale structure and propagation arise because local convection generates a large-scale, asymmetric in the east-west direction, geopotential anomaly that draws warm, moist, conditionally unstable air from the east toward the disturbance. New convection is then triggered on the eastern flank of the existing disturbance, by Kelvin waves and in the real atmosphere by other perturbations, and the pattern becomes organized and bootstraps its way east.

Our results suggest why not all comprehensive, three-dimensional models are able to obtain an MJO. If a model is insufficiently excitable then no convective organization is likely to occur, since the instability is purely local and confined to a column. If a model is too excitable, then convection will be too easily triggered and organization will be hard to achieve. Thus, a convective parameterization that distributes convective effects too smoothly will perforce diminish the gravity wave generation and that excitability. On the other hand, one that produces convection too easily may not lead to a sufficiently coherent structure that is able to propagate eastward, since convection may then also arise west of the coherent structure. Certainly, the nature of the convective parameterization and cloud entrainment parameters do affect the production of an MJO in a GCM (e.g., Holloway et al., 2013; Benedict et al., 2014). Similarly, Klingaman and Woolnough (2014) find that making parameterized convection more sensitive to environmental moisture leads to increased subseasonal variability by delaying the triggering of convection, so allowing moisture anomalies to build for longer periods of time. In particular, forcing convection to prefer more humid environments improves the coherence of the convection and produces greater instability east of the currently active phase, and so an improved MJO simulation. It is precisely the fact that the large-scale moistening and instability occur preferentially east of the existing convection that leads to an eastward propagation in the model we have presented, and without that effect (or if the air to the west of the disturbance is equally unstable) it seems likely that a model would not produce an eastward propagating MJO.

The mechanisms described above seem broadly consistent with the evolution occurring in some more comprehensive 3-D models although the contrasting natures of the models makes comparison difficult. Achieving a better understanding of the connection between them, and the real atmosphere, remains a topic for future work, as is a more complete theoretical exploration of the model we have presented.

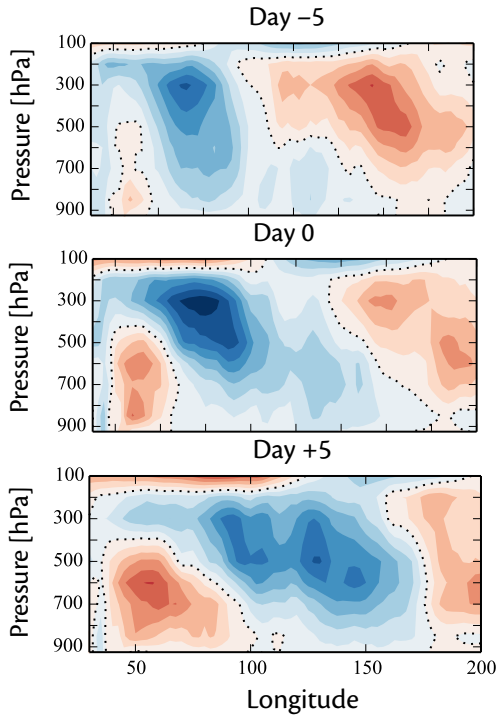

FIGURE 13 Height-longitude section of relative humidity anomaly in a composite MJO in which day 0 has convection peaking over the western Maritime Continent, using ERA-interim reanalysis. Note the tongue of humid air at lower levels east of the main convective region. Analysis courtesy of Prince Xavier.

Acknowledgements

This work was funded by the Leverhulme Trust (RPG-2015-186), NERC (the Paracon Project), and the Newton Fund (CSSP China). We thank Pete Ashwin for conversations about excitable systems, Mat Collins and John Thuburn for general comments about the MJO and convection, Prince Xavier for very graciously providing Fig. 13 and for discussions about GCM simulations of the MJO, and Adam Sobel and an anonymous reviewer for their fine comments.

Appendix: Exact Steady Solutions

In this section we show that the equations of motion admit of steady solutions with no motion, and we find those solutions. Reprising (9), in a state of no motion the height and moisture equations are, neglecting horizontal diffusion,

$$0 = -\gamma C - \lambda_r h, \tag{12a}$$

$$0 = \lambda(q_g - q)\mathcal{H}(q_g - q) - C, \tag{12b}$$

where $\lambda_r = 1/\tau_r$, C is given by (4) and the saturation humidity is given by (7). (We omit the velocity dependence on the evaporation here.)

Suppose first that $q_g \leq q_0$, which we might interpret as being the case with an unsaturated surface. In this case there can only be evaporation if the fluid is sufficiently cold and $h > 0$. However, the radiative forcing and the effects of any condensation will then both warm the fluid and (12a) cannot be satisfied since both terms are negative. The solution in this case is then $h = 0$, $q = q_g$, $C = 0$ (because $q \leq q*$) and zero evaporation. Unless q_g equals q_0 the fluid is not saturated and is stable to infinitesimal perturbations (i.e., perturbations that do not cause saturation); the result of such a perturbation is just a relaxation back to the initial state.

Now suppose $q_g \geq q_0$. A balance can now occur when the evaporation equals the condensation and the radiative cooling equals the latent heat release. Eliminating the condensation term in (12a) and (12b) gives

$$0 = -\lambda_r h - \gamma\lambda(q_g - q)\mathcal{H}(q_g - q). \tag{13}$$

Now, the assumed rapidity of the condensation means that the fluid is, to a very good approximation (asymptotically to $O(\tau)$) saturated and (13) becomes

$$0 = -\lambda_r h - \gamma\lambda\left(q_g - q_0 \exp(-\widehat{\alpha}h)\right), \tag{14}$$

where $\widehat{\alpha} = \alpha/H$ and we omit the Heaviside term since $q_g \geq q$, but retain q_0 for clarity. If $q_g = q_0$ the solution is simply $h = 0$ and $q = q_g$. If $q_g > q_0$ the exact solution of this equation may be written in terms of the Lambert W function, namely the function that satisfies the equation $W(z)\exp(W(z)) = z$ for any z (Corless et al., 1996), with h then given by

$$h = -R + \frac{1}{\widehat{\alpha}} W\left(\frac{\widehat{\alpha}\exp(\alpha R)}{A}\right), \tag{15}$$

where $A = \lambda_r/(\gamma\lambda q_0)$ and $R = q_g\gamma\lambda/\lambda_r$. This solution is the shallow water analog of the drizzle solution in the vertically continuous problem found by Vallis et al. (2019), and the precipitation in both cases is non-convective, involving no fluid motion.

A more easily interpreted expression results if we suppose that the saturation humidity varies linearly with the height field and $q^* = q_0(1 - \widehat{\alpha}h)$. Equation (14) becomes

$$0 = -\lambda_r h - \gamma\lambda\left(q_g - q_0(1 - \widehat{\alpha}h)\right) \tag{16}$$

with solution

$$h = \frac{-\gamma\lambda(q_g - q_0)}{\lambda_r + \gamma\lambda q_0\widehat{\alpha}}, \tag{17}$$

and the humidity is the saturated value occurring at this value. If $q_g = q_0$ then $h = 0$, as expected, giving a solution with no evaporation or precipitation. If $q_g > q_0$ then evaporation occurs, warming the fluid and reducing the value of h. The humidity, q, is then less than that at the surface, q_g, and evaporation is continuous. In the steady state the resulting value of h is such that the evaporation exactly replenishes the condensation, and the condensational heating is exactly balanced by the

radiative cooling. For $q_g = 1.1q_0$ and the other parameters taking the values previously derived, (17) gives values of h of order 0.1 m or less, considerably smaller than the variations we will find when the model is in a convective regime.

More than their particular form, the expression (15) and its approximation (17) are important because they demonstrate that steady solutions of no motion do exist to the problem.

REFERENCES

Adames, Á. F. and Wallace, J. M. (2014) Three-dimensional structure and evolution of the MJO and its relation to the mean flow. *J. Atmos. Sci.*, **71**, 2007–2026.

Arakawa, A. and Schubert, W. H. (1974) Interaction of a cumulus cloud ensemble with the large-scale environment, part i. *J. Atmos. Sci.*, **31**, 674–701.

Arnold, N. P. and Randall, D. A. (2015) Global-scale convective aggregation: Implications for the Madden–Julian Oscillation. *J. Adv. Model. Earth Sys.*, **7**, 1499–1518.

Benedict, J. J., Maloney, E. D., Sobel, A. H. and Frierson, D. M. (2014) Gross moist stability and MJO simulation skill in three full-physics GCMs. *J. Atmos. Sci.*, **71**, 3327–3349.

Betts, A. K. (1973) Non-precipitating convection and its parameterization. *Quart. J. Roy. Meteor. Soc.*, **99**, 178–196.

— (1986) A new convective adjustment scheme. Part I: Observational and theoretical basis. *Quart. J. Roy. Meteor. Soc.*, **112**, 677–691.

Biello, J. A. and Majda, A. J. (2005) A new multiscale model for the Madden–Julian oscillation. *J. Atmos. Sci.*, **62**, 1694–1721.

Bouchut, F., Lambaerts, J., Lapeyre, G. and Zeitlin, V. (2009) Fronts and nonlinear waves in a simplified shallow-water model of the atmosphere with moisture and convection. *Phys. Fluids*, **21**, 116604.

Bretherton, C. S., Blossey, P. N. and Khairoutdinov, M. (2005) An energy-balance analysis of deep convective self-aggregation above uniform sst. *J. Atmos. Sci.*, **62**, 4273–4292.

Corless, R. M., Gonnet, G. H., Hare, D. E., Jeffrey, D. J. and Knuth, D. E. (1996) On the LambertW function. *Adv. Comp. Math.*, **5**, 329–359.

De Szoeke, S. P., Edson, J. B., Marion, J. R., Fairall, C. W. and Bariteau, L. (2015) The MJO and air–sea interaction in TOGA COARE and DYNAMO. *J. Climate*, **28**, 597–622.

DeMott, C. A., Klingaman, N. P. and Woolnough, S. J. (2015) Atmosphere-ocean coupled processes in the Madden–Julian oscillation. *Rev. Geophys.*, **53**, 1099–1154.

Emanuel, K. A., Fantini, M. and Thorpe, A. J. (1987) Baroclinic instability in an environment of small stability to slantwise moist convection. Part I: Two-dimensional models. *J. Atmos. Sci.*, **44**, 1559–1573.

Emanuel, K. A., Neelin, J. D. and Bretherton, C. S. (1994) On large-scale circulations in convecting atmospheres. *Quart. J. Roy. Meteor. Soc.*, **120**, 1111–1143.

Frierson, D. M., Majda, A. J. and Pauluis, O. M. (2004) Large scale dynamics of precipitation fronts in the tropical atmosphere: A novel relaxation limit. *Comm. Math. Sci.*, **2**, 591–626.

Fuchs, Z. and Raymond, D. J. (2017) A simple model of intraseasonal oscillations. *J. Adv. Model. Earth Sys.*, **9**, 1195–1211.

Gill, A. E. (1980) Some simple solutions for heat induced tropical circulation. *Quart. J. Roy. Meteor. Soc.*, **106**, 447–462.

Hastenrath, S. and Polzin, D. (2004) Dynamics of the surface wind field over the equatorial Indian Ocean. *Quart. J. Roy. Meteor. Soc.*, **130**, 503–517.

Heckley, W. and Gill, A. (1984) Some simple analytical solutions to the problem of forced equatorial long waves. *Quart. J. Roy. Meteor. Soc.*, **110**, 203–217.

Holloway, C. E., Woolnough, S. J. and Lister, G. M. (2013) The effects of explicit versus parameterized

convection on the MJO in a large-domain high-resolution tropical case study. Part I: Characterization of large-scale organization and propagation. *J. Atmos. Sci.*, **70**, 1342–1369.

Izhikevich, E. M. (2007) *Dynamical Systems in Neuroscience: the Geometry of Excitability and Bursting*. MIT Press.

Khairoutdinov, M. F. and Emanuel, K. (2018) Intraseasonal variability in a cloud-permitting near-global equatorial aquaplanet model. *J. Atmos. Sci.*, **75**, 4337–4355.

Kiladis, G. N., Straub, K. H. and Haertel, P. T. (2005) Zonal and vertical structure of the Madden–Julian oscillation. *J. Atmos. Sci.*, **62**, 2790–2809.

Kiladis, G. N., Wheeler, M. C., Haertel, P. T., Straub, K. H. and Roundy, P. E. (2009) Convectively coupled equatorial waves. *Rev. Geophys.*, **47**, RG2003.

Klingaman, N. and Woolnough, S. (2014) Using a case-study approach to improve the Madden–Julian oscillation in the Hadley Centre model. *Quart. J. Roy. Meteor. Soc.*, **140**, 2491–2505.

Lambaerts, J., Lapeyre, G. and Zeitlin, V. (2011) Moist versus dry barotropic instability in a shallow-water model of the atmosphere with moist convection. *J. Atmos. Sci.*, **68**, 1234–1252.

Lau, W. K.-M. and Waliser, D. E. (2012) *Intraseasonal variability in the atmosphere-ocean climate system*. Springer, 2nd edn.

Liu, P., Satoh, M., Wang, B., Fudeyasu, H., Nasuno, T., Li, T., Miura, H., Taniguchi, H., Masunaga, H., Fu, X. et al. (2009) An MJO simulated by the NICAM at 14- and 7-km resolutions. *Mon. Wea. Rev.*, **137**, 3254–3268.

Madden, R. A. and Julian, P. R. (1971) Detection of a 40–50 day oscillation in the zonal wind in the tropical Pacific. *J. Atmos. Sci.*, **28**, 702–708.

Majda, A. J. and Stechmann, S. N. (2009) The skeleton of tropical intraseasonal oscillations. *Proc. Nat. Acad. Sci.*, **106**, 8417–8422.

Matsuno, T. (1966) Quasi-geostrophic motions in the equatorial area. *J. Meteor. Soc. Jpn.*, **44**, 25–43.

Meron, E. (1992) Pattern formation in excitable media. *Phys. Rep.*, **218**, 1–66.

Muller, C. and Bony, S. (2015) What favors convective aggregation and why? *Geophys. Res. Lett.*, **42**, 5626–5634.

Nasuno, T., Miura, H., Satoh, M., Noda, A. T. and Oouchi, K. (2009) Multi-scale organization of convection in a global numerical simulation of the December 2006 MJO event using explicit moist processes. *J. Meteor. Soc. Jpn.*, **87**, 335–345.

Neelin, J. D., Held, I. M. and Cook, K. H. (1987) Evaporation-wind feedback and low-frequency variability in the tropical atmosphere. *J. Atmos. Sci.*, **44**, 2341–2348.

Raymond, D. J. (2001) A new model of the Madden–Julian oscillation. *J. Atmos. Sci.*, **58**, 2807–2819.

Raymond, D. J. and Fuchs, Ž. (2009) Moisture modes and the Madden–Julian oscillation. *J. Climate*, **22**, 3031–3046.

Rostami, M. and Zeitlin, V. (2018) An improved moist-convective rotating shallow-water model and its application to instabilities of hurricane-like vortices. *Quart. J. Roy. Meteor. Soc.*, **144**, 1450–1462.

Sobel, A. and Maloney, E. (2013) Moisture modes and the eastward propagation of the MJO. *J. Atmos. Sci.*, **70**, 187–192.

Sobel, A. H., Nilsson, J. and Polvani, L. (2001) The weak temperature gradient approximation and balanced tropical moisture waves. *J. Atmos. Sci.*, **58**, 3650–3665.

Vallis, G. K. (2017) *Atmospheric and Oceanic Fluid Dynamics*. Cambridge, U.K.: Cambridge University Press, 2nd edn.

Vallis, G. K., Parker, D. J. and Tobias, S. M. (2019) A simple system for moist convection: the Rainy–Bénard model. *J. Fluid Mech.*, **862**, 162–199.

Wang, B., Chen, G. and Liu, F. (2019) Diversity of the Madden-Julian oscillation. *Sci. Adv.*, **5**, 8 pages.

Wheeler, M. and Kiladis, G. N. (1999) Convectively coupled equatorial waves: Analysis of clouds and temperature in the wavenumber-frequency domain. *J. Atmos. Sci.*, **56**, 374–399.

Wing, A. A., Emanuel, K., Holloway, C. E. and Muller, C. (2017) Convective self-aggregation in numerical simulations: A review. In *Shallow Clouds, Water Vapor, Circulation, and Climate Sensitivity*, 1–25. Springer.

Würsch, M. and Craig, G. C. (2014) A simple dynamical model of cumulus convection for data assimilation research. *Meteor. Zeit.*, **5**, 483–490.

Xu, K.-M. and Emanuel, K. A. (1989) Is the tropical atmosphere conditionally unstable? *Mon. Wea. Rev.*, **117**, 1471–1479.

Yang, D. and Ingersoll, A. P. (2013) Triggered convection, gravity waves, and the MJO: A shallow-water model. *J. Atmos. Sci.*, **70**, 2476–2486.

Yano, J.-I., McWilliams, J. C. and Moncrieff, M. W.and Emanuel, K. A. (1995) Hierarchical tropical cloud systems in an analog shallow-water model. *J. Atmos. Sci.*, **52**, 1723–1742.

Zhang, C. (2005) Madden–Julian oscillation. *Rev. Geophys.*, **43**, 1–36.

The End.

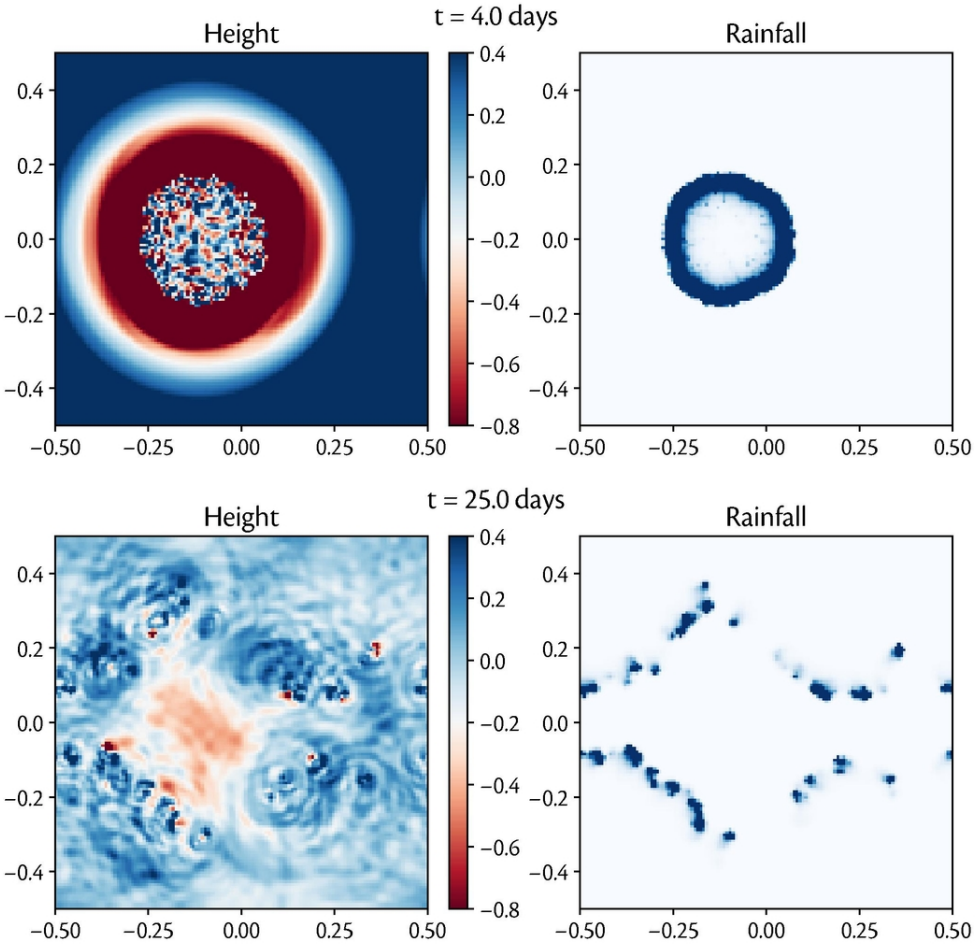

1 Snapshots of the height and precipitation fields at the times indicated, following an initial small perturbation at y = 0 and x = −0.1. (Units of x and y are 107 m, and the precipitation field is slightly smoothed in space and time and uses a near-binary colour map.) The disturbance generates a front that propagates away from the disturbance before breaking up, then continuing in excitable, self-sustained motion.
By time 25 the precipitation fronts are propagating quasi-randomly though the domain, breaking up and reforming every several days.

90x87mm (300 x 300 DPI)

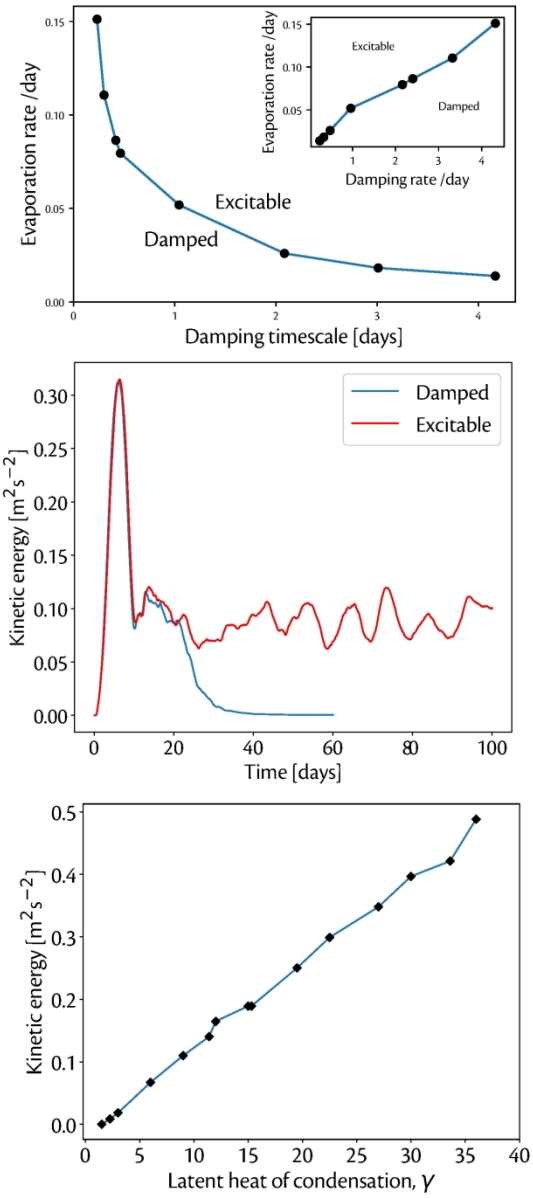

2 (a) Boundary of the excitable state for varying values of the radiative damping of the height field and the efficiency of evaporation. The stationary state is saturated with no precipitation of evaporation. In the excitable regime the system maintains a chaotic, convectively active state. In the stable state the system eventually returns to its original state of no motion, even though that state is linearly unstable. (b) Evolution in excitable and a damped states, both with a damping timescale of 2 days and with evaporative parameters on either side of the critical line. (c) The domain
and time-averaged kinetic energy as a function of the latent heat parameter, γ

122x271mm (300 x 300 DPI)

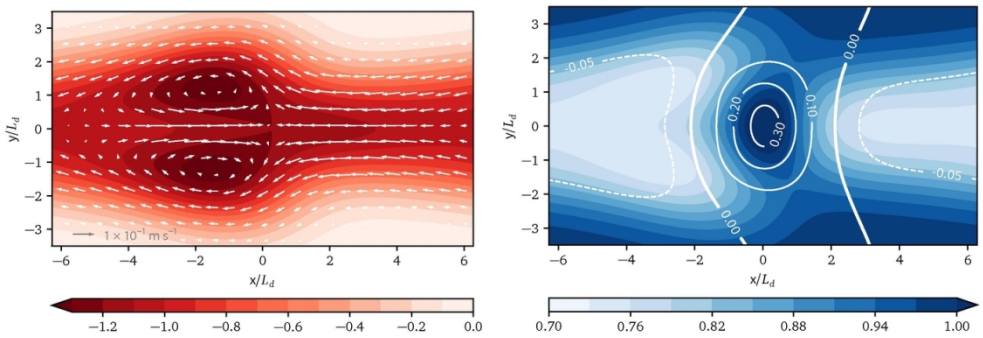

3 Response to a steady heating centered at the origin on an equatorial beta-plane, where moisture is a passive tracer. (a) The height field (color filled contours) and wind vectors (arrows). (b) The absolute humidity (specifically $q/q_0 - 1$, white contours) and relative humidity q/q_* (color filled contours), with darkest blue
indicating saturation.

120x42mm (300 x 300 DPI)

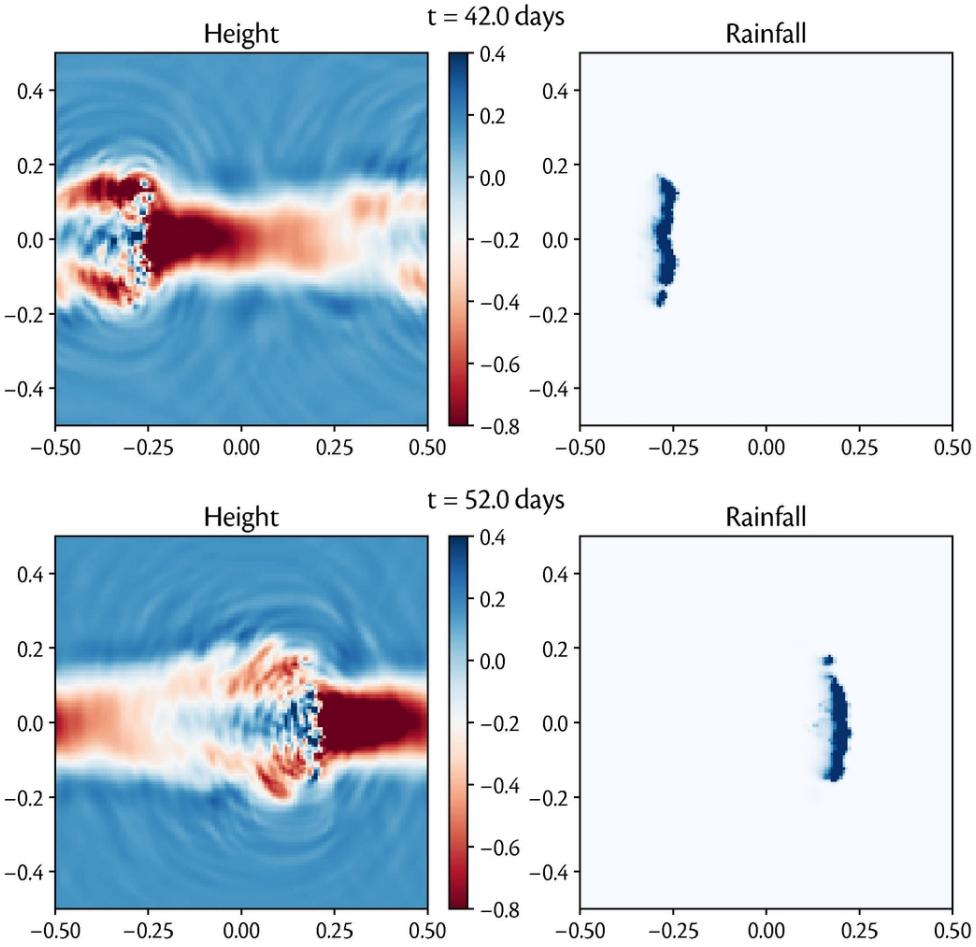

4 Snapshots of the height and precipitation fields at the times indicated, in simulations on a beta plane, with β = 2 × 10−11 m1 s−1, a resolution of 25 km and no imposed mean flow. The main disturbance forms about 30 days after initialization and propagates eastward at about 6 m s−1. Units of x and y are 107 m and the equatorial
deformation radius is about 106 m

90x87mm (300 x 300 DPI)

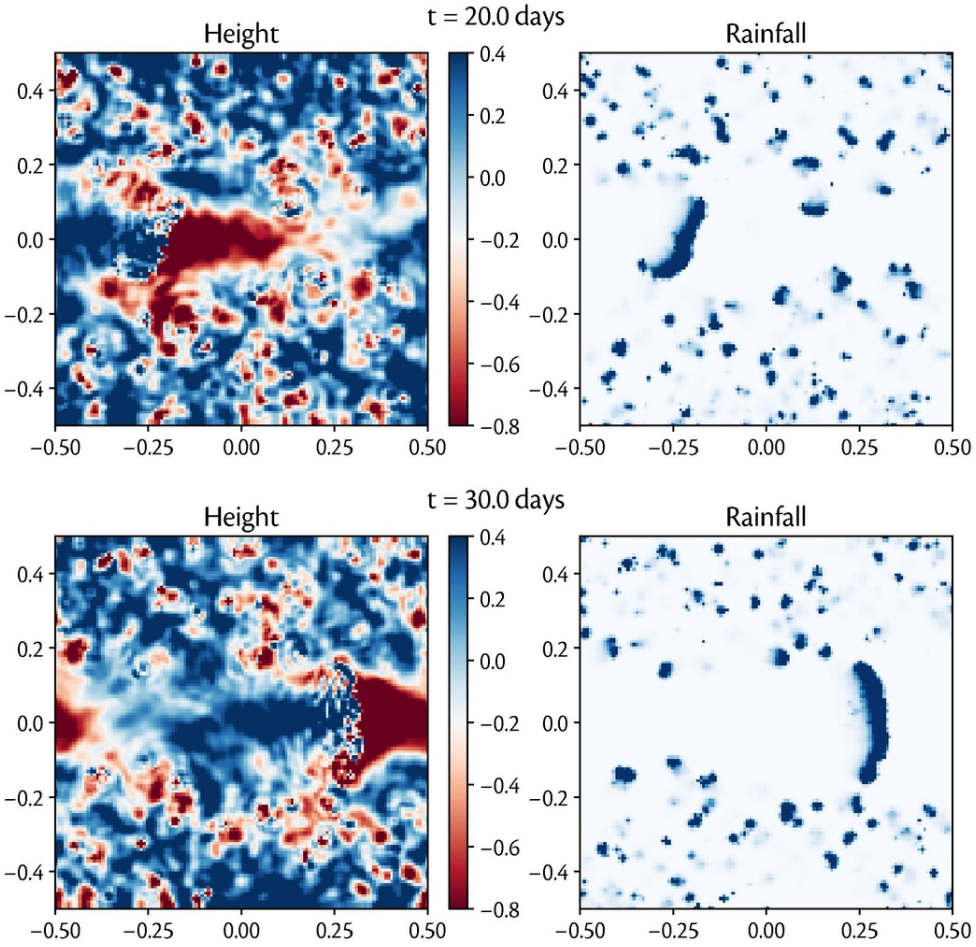

5 As for Fig. 4 except that a mean westward flow of 1 m s−1 is included in the bulk-aerodynamic formulation of evaporation

90x87mm (300 x 300 DPI)

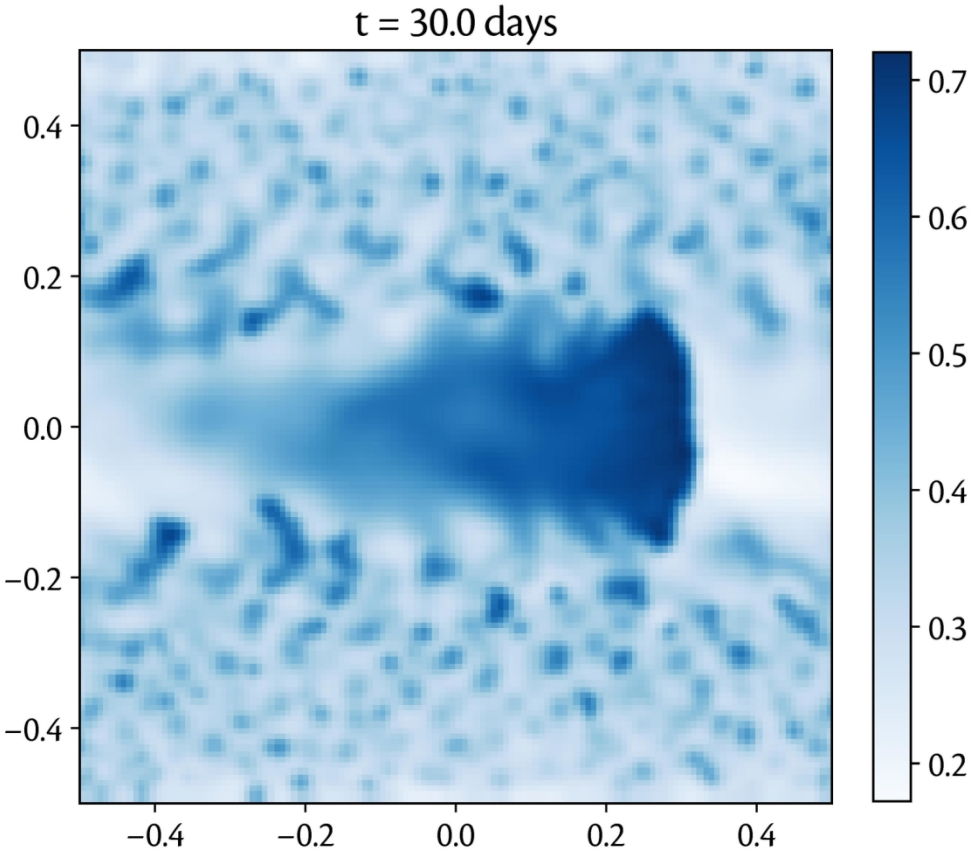

6 Snapshot of evaporation field (normalized by its maximum value) in the simulation of Fig. 5. The evaporation is less ahead of (i.e. east of) the main convective region

142x125mm (300 x 300 DPI)

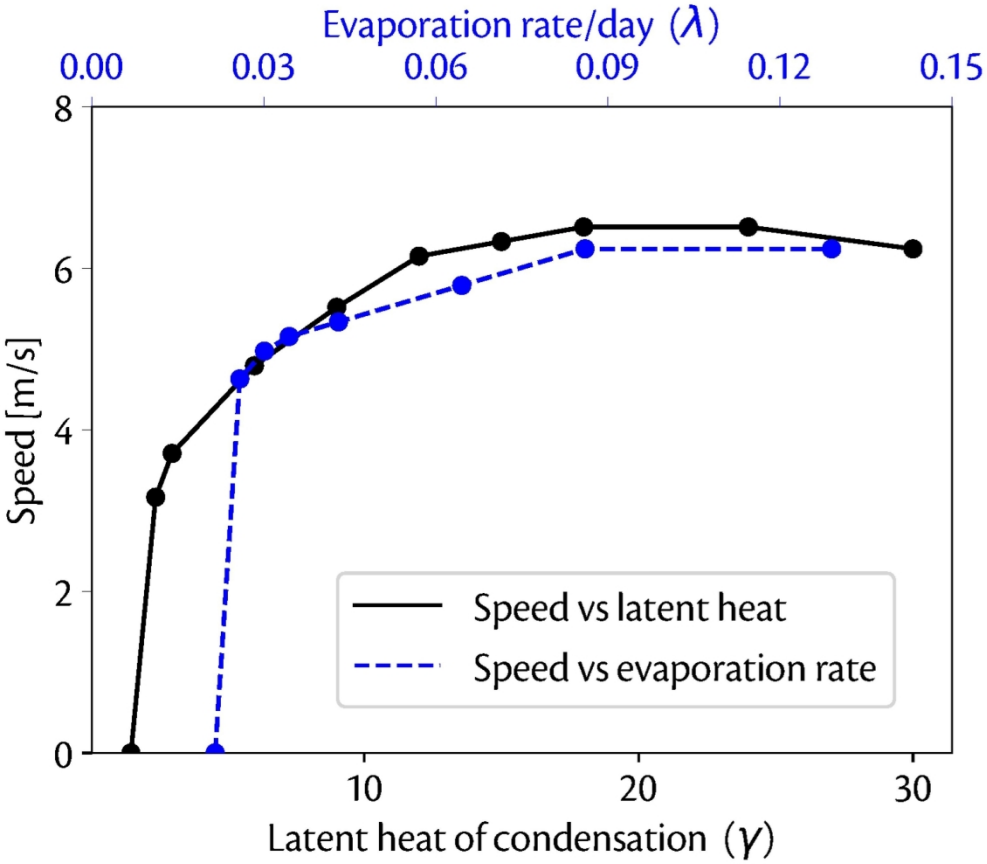

7 Speed of the main, MJO-like, eastward moving disturbance as function of the evaporation coefficient λ and the latent heat of condensation, γ. Where γ varies the value of λ is fixed at 0.08 and when λ varies the value of γ is 15.

132x116mm (300 x 300 DPI)

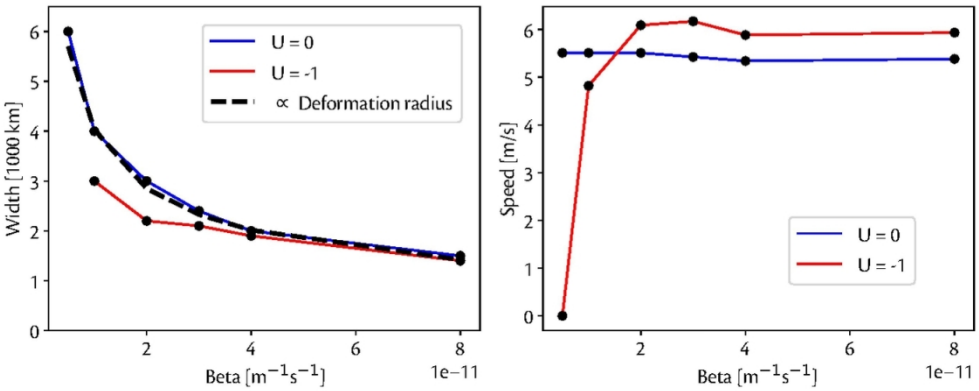

8 (a) Width of the precipitating region as a function of β. The deformation radius, c/2β is about 700 km in the these experiments. The two solid curves show a sequence of experiments with U = 0 and U = −1 m s−1, where U is the speed of the imposed mean flow affecting the evaporation. The dashed line shows a curve proportional to β−1/2. (b) Same as (a), except now for the speed of the disturbance. For β = 0.5 × 10−11 no MJO-like phenomena is obtained in the case with U = −1.

120x49mm (300 x 300 DPI)

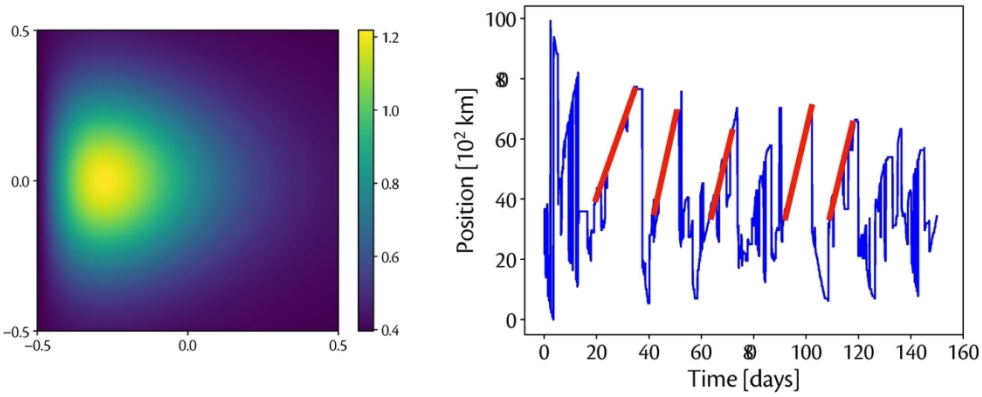

9 (a) Sea-surface humidity, representing a warm pool in the western equatorial region with a fractional humidity about 25% above a base level (b) Position of the maximum precipitation at the equator, with thicker red lines indicating where the precipitation is associated with MJO-like activity. MJO events form only in the warm western
region and decay before reaching the eastern edge, and here recur every 20–40 days

126x52mm (300 x 300 DPI)

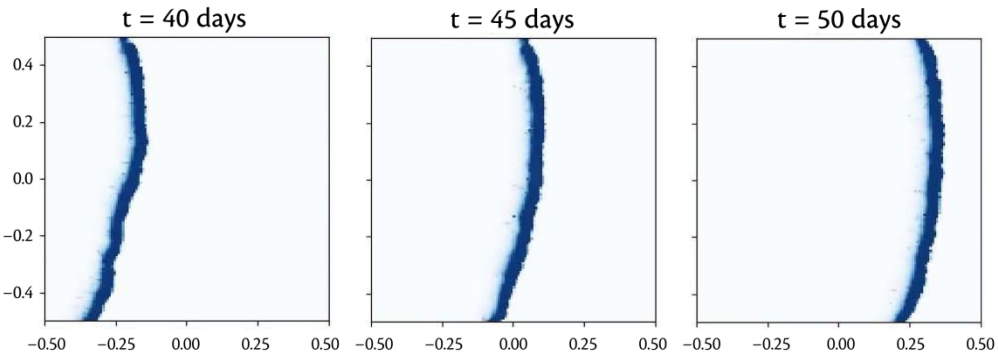

10 Rainfall at the times indicated in a simulation with no rotation, f = β = 0, but with an imposed uniform westward mean flow of 1 m s−1 in the bulk formula for the evaporation, (11). This term is the only one in the system that imposes a mean
direction. The speed of the front here is about 5 m s−1

330x116mm (300 x 300 DPI)

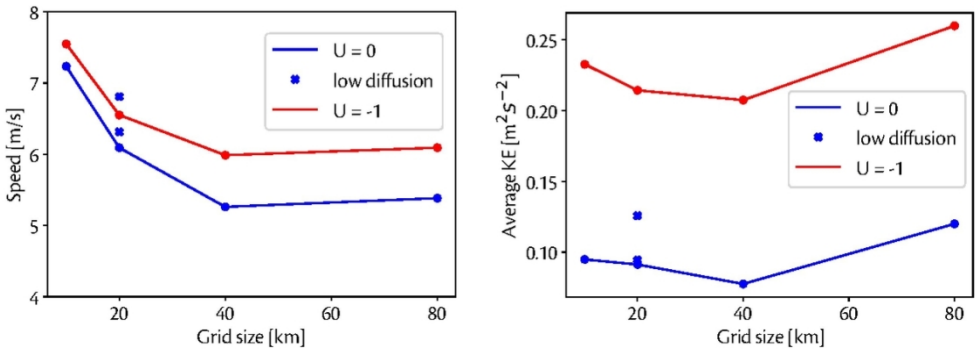

11 (a) Dependence on resolution of the speed of the moving disturbance. (b) Dependence on resolution of average kinetic energy of the system (over the whole domain). The blue and red lines show simulations without and with an additional mean westward flow of 1 m s−1 affecting the evaporation. The additional cross marks show simulations with values of the diffusivity of height, moisture and velocity further reduced by factors of 2 and 4, in simulations without the additional wind-induced evaporation.

111x41mm (300 x 300 DPI)

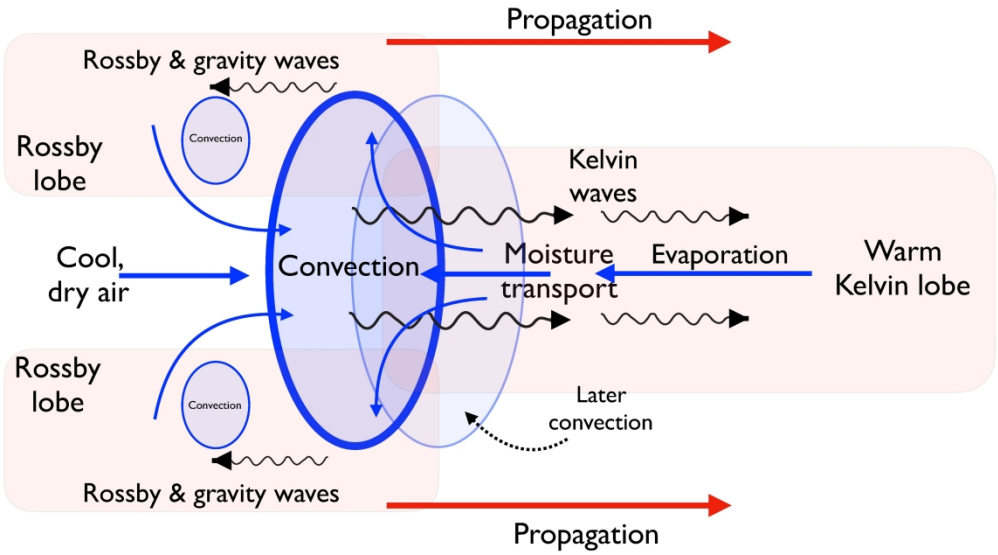

12 Schematic of an eastward propagating equatorial disturbance. Convection at the equator gives rise to a feedback producing convective organization and a modified Matsuno– Gill-like pattern. Warm moist air is then drawn in from the east but this is convectively unstable, amenable to triggering by the eastward propagating gravity waves from the initial disturbance, and new convection forms on the eastern edge of the original location. The whole pattern then moves unsteadily eastward.

371x204mm (300 x 300 DPI)

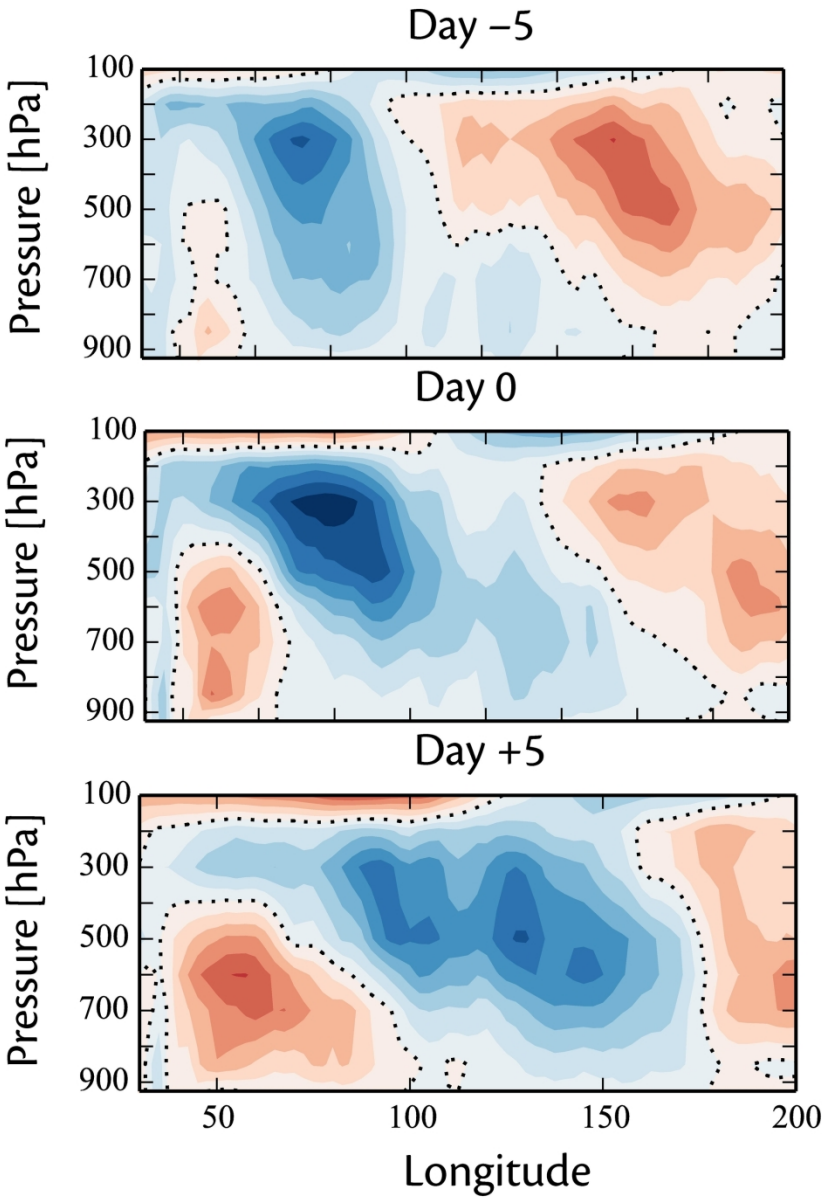

13 Height-longitude section of relative humidity anomaly in a composite MJO in which day 0 has convection peaking over the western Maritime Continent, using ERA-interim reanalysis. Note the tongue of humid air at lower levels east of the
main convective region. Analysis courtesy of Prince Xavier

172x249mm (300 x 300 DPI)